

Luminark: Training-free, Probabilistically-Certified Watermarking for General Vision Generative Models

Jiayi Xu ^{*1} Zhang Zhang ^{*1} Yuanrui Zhang ¹ Ruitao Chen ¹ Yixian Xu ¹ Tianyu He ² Di He ¹

Abstract

In this paper, we introduce *Luminark*, a training-free and probabilistically-certified watermarking method for general vision generative models. Our approach is built upon a novel watermark definition that leverages patch-level luminance statistics. Specifically, the service provider predefines a binary pattern together with corresponding patch-level thresholds. To detect a watermark in a given image, we evaluate whether the luminance of each patch surpasses its threshold and then verify whether the resulting binary pattern aligns with the target one. A simple statistical analysis demonstrates that the false positive rate of the proposed method can be effectively controlled, thereby ensuring certified detection. To enable seamless watermark injection across different paradigms, we leverage the widely adopted guidance technique as a plug-and-play mechanism and develop the *watermark guidance*. This design enables *Luminark* to achieve generality across state-of-the-art generative models without compromising image quality. Empirically, we evaluate our approach on nine models spanning diffusion, autoregressive, and hybrid frameworks. Across all evaluations, *Luminark* consistently demonstrates high detection accuracy, strong robustness against common image transformations, and good performance on visual quality.

1. Introduction

Watermarking has long served as a key technique for protecting digital content in computer vision. With the rise of AI-generated media, its importance has increased substantially, driven by the increasing risks of misuse and unauthorized redistribution. However, designing a general-purpose watermarking method for vision generative models remains a significant challenge. The main difficulty arises from the diver-

¹Peking University, Beijing, China ²Microsoft Research Asia, Beijing, China. Correspondence to: Di He <dihe@pku.edu.cn>.

Preprint. January 6, 2026.

sity of modern generative modeling paradigms in computer vision—ranging from diffusion-based frameworks (Ho et al., 2020; Song et al., 2020a; Lipman et al., 2022; Song et al., 2023) to autoregressive(AR) models (Tian et al., 2024; Li et al., 2024)—each of which follows distinct design principles, neural network architectures, training objectives, and inference procedures.

Classical approaches embed signatures into the images' frequency coefficients (Cox et al., 1997; Bi et al., 2007; Hsieh et al., 2001; Pereira & Pun, 2000; Potdar et al., 2005). Although broadly applicable, these methods suffer from limited robustness against common image transformations. Recently, a line of works has explored *neural-network-based approaches*, which either fine-tune the generative model's parameters to synthesize watermarked output (Zhao et al., 2023; Fernandez et al., 2023; Min et al., 2024) or train separate neural networks for watermark injection and detection (Bui et al., 2023; Lu et al., 2024; Sander et al., 2024). With careful data augmentation, these methods can achieve substantial robustness and maintain high perceptual quality. However, the black-box nature of neural networks provides no theoretical guarantees on detection reliability—users cannot rigorously evaluate when or why detection might fail, nor estimate the likelihood of such failures. Another line of work has proposed *probabilistically-certified approaches* that offer formal statistical guarantees for detection (Wen et al., 2023; Jovanović et al., 2025). Nevertheless, these methods are typically tailored to a specific generative paradigm and, according to our experiments, introduce degradation in image quality.

In this paper, we introduce **Luminark**, a new path to probabilistically-certified watermarking that (i) offers a strong statistical guarantee for detection, (ii) substantially outperform prior probabilistically-certified methods on the generation quality, (iii) remains robust against a variety of image transformations, and (iv) achieves this in a training-free, plug-and-play manner applicable to diverse generative paradigms. Our first contribution is the introduction of a novel watermark for image protection. Given an image, we partition it into patches and compute the luminance value of each patch. The watermark is defined as a binary pattern over these luminance values—whether each patch's luminance exceeds a specified threshold. We mathematically



Figure 1. Luminark on Stable Diffusion 2.1. Left: unwatermarked output. Right: watermarked output.

show that if the binary pattern and thresholds are randomly chosen, the probability that an unwatermarked image (e.g., a natural image) matches the pattern decreases exponentially with respect to the number of patches, thereby making reliable detection feasible (*supporting (i)*). Moreover, since detection relies solely on patch-level statistics, it remains robust against common image transformations (*supporting (iii)*), such as smoothing, quantization, and compression.

From the service provider’s perspective, although detection in Luminark is straightforward, injecting the predefined pattern and maintaining high-quality generation is considerably more challenging. The second contribution of our work is the design of a training-free injection algorithm that enables Luminark to operate across diverse generative paradigms and generate visually convincing outputs. The key insight is that all recent generative paradigms, despite their differences, share a common mechanism—the guidance technique (Dhariwal & Nichol, 2021; Ho & Salimans, 2022; Karras et al., 2024a). Guidance has become a standard tool in both diffusion and autoregressive vision models, where it enhances output quality by steering the generation process toward desired outcomes. We leverage this mechanism as the entry point for watermark injection (*supporting (iv)*) and introduce *the watermark guidance*, which directs each generation step toward alignment with the predefined pattern. This enables the watermark to be softly injected into the generation process in a plug-and-play manner, while simultaneously adjusting the content smoothly to preserve the quality of the generated image.

We conduct extensive experiments to evaluate the effectiveness of Luminark. Specifically, we test Luminark on diffusion models, autoregressive models, and hybrid solutions, including EDM2 (Karras et al., 2024b), Stable Diffusion (Rombach et al., 2022), VAR (Tian et al., 2024), and MAR (Li et al., 2024), spanning model scales from a few hundred million to several billion parameters, covering diverse neural architectures (continuous and discrete tokenizers, U-Nets and Transformers), different output resolutions (256×256 , 512×512 and 768×768) and applications (vanilla class-conditional image generation and text-to-image generation). Experimental results demonstrate that Luminark largely outperforms previous probabilistically-certified baselines and preserves perceptual quality (*supporting (ii)*), while simultaneously achieving high detection rates against common image transformations. These results establish Luminark as a practical and general-purpose watermarking algorithm for vision generative models.

2. Related Works

Existing watermarking approaches in vision can be broadly classified into three distinct lines: classical post-hoc watermarking, neural-network-based watermarking, and probabilistically-certified watermarking.

Classical post-hoc watermarking refers to early approaches that inject a watermark into an image post hoc. To ensure imperceptibility, these methods typically transform the image into the frequency domain and adjust specific frequency coefficients to encode a signature (Bi et al.,

2007; Hsieh et al., 2001; Pereira & Pun, 2000; Potdar et al., 2005). However, these approaches face a crucial trade-off between maintaining image quality and achieving robustness. Modifying low-frequency coefficients often leads to noticeable degradation in image quality, whereas modifying high-frequency coefficients makes the detection vulnerable to local perturbations (Cox et al., 2007). Owing to its efficiency and model-agnostic nature, this approach remains widely used, including in systems such as Stable Diffusion (Rombach et al., 2021).

Neural-network-based watermarking. These approaches typically involve training a neural network to determine whether a query image contains a watermark. Regarding watermark injection, existing strategies generally follow three paradigms: some methods fine-tune the generative model itself, enabling it to synthesize watermarked content directly (Zhao et al., 2023; Fernandez et al., 2023; Min et al., 2024; Wang et al., 2025); some methods utilize multiple techniques to fuse the watermark during generation without modifying the model parameters (Gesny et al., 2025; Fares et al., 2025), such as training a plug-and-play "adapter" (Ci et al., 2024a; Zhang et al., 2025); while others train a separate neural network as a post-hoc watermark injector (Bui et al., 2023; Lu et al., 2024; Sander et al., 2024; Huang et al., 2025; Gowal et al., 2025; Evennou et al., 2025; Souček et al., 2025; Choi et al., 2025; Fairoze et al., 2025). With careful data augmentations, these methods can achieve strong perceptual quality while maintaining detection robustness under common image distortions. However, owing to the inherent black-box nature of these models, users cannot rigorously evaluate when or why detection might fail, nor assess the reliability of a given detection outcome.

Probabilistically-certified watermarking injects a chosen random perturbation into the generative process so that the resulting distribution of outputs carries a statistically testable signal. Detection is then cast as a hypothesis test, checking whether a sample originates from the perturbed (watermarked) distribution rather than the original one. The test itself is typically tailored to the generative paradigm: diffusion models permit testing for structured patterns in the recovered noise, while autoregressive models test for distributional shifts in token statistics. As a result, different architectures require different perturbations and, consequently, different statistical tests. The pioneering work in this domain is the Tree-Ring watermark (Wen et al., 2023), which embeds a pattern into the initial noise vector of diffusion models. Detection is performed by inverting the generation process (via inverse ODE solvers) to recover the noise and verifying its alignment with the embedded pattern. Subsequent works have refined this concept with advanced designs (Yang et al., 2024; Ci et al., 2024b; Gunn et al., 2024; Huang et al., 2024; Arabi et al., 2024; Yang et al., 2025; Lee & Cho, 2025; Zhang et al., 2024; Mao et al.,

2025). Recently, probabilistically-certified methods have also been proposed for autoregressive models (Jovanović et al., 2025; Kerner et al., 2025), but these methods remain tightly coupled to specific generative paradigms. This architecture dependency limits their universality, and their visual fidelity remains considerably lower than neural-network-based watermarking approaches.

3. Watermarking as Luminance Constraints

3.1. Watermark Definition

In this work, we explore a novel watermarking mechanism for general image generation based on patch-level luminance statistics. In computer vision, *luminance* refers to the perceived brightness of a pixel, derived from its RGB values (Szeliski, 2022; Gonzalez & Woods, 2018). It represents the grayscale intensity that a human observer would perceive from a colored image.

Mathematically, we first partition an image \mathbf{x} of size $H \times W$ into non-overlapping patches of size $k \times k$, i.e., $\mathbf{x} = \{\mathbf{p}_1, \mathbf{p}_2, \dots, \mathbf{p}_N\}$, where \mathbf{p}_1 denotes the patch in the top-left corner and \mathbf{p}_N corresponds to the patch in the bottom-right corner. The total number of patches N is given by $\frac{H \times W}{k^2}$. For each patch \mathbf{p}_i , we compute the average pixel values (normalized into $(0, 1)$ in the R, G, and B channels, denoted as $(\bar{R}_i, \bar{G}_i, \bar{B}_i)$. The luminance of the patch is then defined as:

$$l(\mathbf{p}_i) = 0.299 \cdot \bar{R}_i + 0.587 \cdot \bar{G}_i + 0.114 \cdot \bar{B}_i. \quad (1)$$

We denote the luminance of \mathbf{x} as vector $\mathbf{L}(\mathbf{x}) = (l(\mathbf{p}_1), l(\mathbf{p}_2), \dots, l(\mathbf{p}_N))$. To avoid confusion, we denote the generated and real images as \mathbf{x}_{gen} and \mathbf{x}_{real} , respectively. Our goal is to inject specific patterns (i.e., signature) into the generation process of \mathbf{x}_{gen} such that its luminance $\mathbf{L}(\mathbf{x}_{\text{gen}})$ becomes statistically distinguishable from that of the real image \mathbf{x}_{real} , thereby enabling watermark detection. To construct this statistical difference, we first define a binary pattern $\mathbf{c} = (c_1, c_2, \dots, c_N) \in \{-1, 1\}^N$ and a real-valued threshold vector $\boldsymbol{\tau} = (\tau_1, \tau_2, \dots, \tau_N) \in (0, 1)^N$. Both values in \mathbf{c} and $\boldsymbol{\tau}$ can be randomly generated using a pseudo-random number generator, fixed by the service provider, and are not released to the web users.

The real-valued vector $\boldsymbol{\tau}$ is used to access the “level” of luminance. For each patch i , we compute a decision stump of the form $\text{sgn}[l(\mathbf{p}_i) - \tau_i]$, which evaluates whether the patch’s luminance exceeds τ_i . The sign function $\text{sgn}(\cdot)$ returns the sign of a real number, outputting -1 for negative inputs, and $+1$ for non-negative inputs. Applying this across all patches yields the binary pattern of \mathbf{x} :

$$\mathbf{o}(\mathbf{x}) = (\text{sgn}[l(\mathbf{p}_1) - \tau_1], \dots, \text{sgn}[l(\mathbf{p}_N) - \tau_N]) \in \{-1, 1\}^N.$$

Detection is performed by comparing the similarity of the

binary pattern of the image $\mathbf{o}(\mathbf{x})$ and the predefined \mathbf{c} . Intuitively, if both \mathbf{c} and τ are randomly selected and known only to the provider, a natural image is unlikely to match the pattern by chance. Therefore, if the image pattern $\mathbf{o}(\mathbf{x})$ sufficiently differs from \mathbf{c} , the image \mathbf{x} is identified to be unwatermarked. A statistical analysis and a more rigorous detection algorithm are presented in Section 3.2.

For completeness, we denote a watermark $\mathcal{W} = (\mathbf{c}, \tau)$. This approach offers several key advantages. First and most notably, the watermark is designed to be imperceptible to humans, as it operates on the average luminance of each patch rather than injecting pixel-level patterns. Furthermore, the use of patch-level average luminance as the signature provides inherent robustness against several popularly studied image manipulations. The averaging calculation acts as a low-pass filter, making the signature resilient to random perturbations like added noise or artifacts from mild compression. Such modifications are unlikely to alter the average luminance of a patch enough to flip its outcome relative to the threshold, thus preserving the integrity of the watermark.

3.2. Probabilistically-Certified Watermark Detection

The objective of watermark detection is to reliably determine whether a given query image \mathbf{x} has been injected with a specific predefined watermark. We begin by defining the core metric for our test. For a given image \mathbf{x} and watermark $\mathcal{W} = (\mathbf{c}, \tau)$, recall that \mathbf{x} is partitioned into N patches $\{\mathbf{p}_i\}_{i=1}^N$. We define the **match rate**, $m(\mathbf{x}, \mathcal{W})$, as fraction of patches whose luminance statistics align with the watermark's binary pattern \mathbf{c} :

$$m(\mathbf{x}, \mathcal{W}) = \frac{1}{N} \sum_{i=1}^N \mathbb{I}[\text{sgn}(l(\mathbf{p}_i) - \tau_i) = c_i] \quad (2)$$

where $\mathbb{I}[\cdot]$ is the indicator function.

We next show that, for an unwatermarked (e.g., natural) image, its match rate can be well controlled with high probability if \mathcal{W} is randomly chosen.

Proposition 1. *Assume each c_i is drawn i.i.d from $\text{Bernoulli}(\frac{1}{2})$ with support $\{-1, 1\}$ and each τ_i is drawn i.i.d from any distribution with support $(0, 1)$, then for any fixed \mathbf{x} , for any $0 \leq \varepsilon \leq \frac{1}{2}$, we have*

$$\begin{aligned} \Pr\left(m(\mathbf{x}, \mathcal{W}) \geq \frac{1}{2} + \varepsilon\right) &= \frac{1}{2^N} \sum_{k=\lceil N(\frac{1}{2} + \varepsilon) \rceil}^N \binom{N}{k} \quad (3) \\ &\leq \exp(-N \cdot D_{KL}(\varepsilon)) \quad (4) \end{aligned}$$

where $D_{KL}(\varepsilon) = (\frac{1}{2} + \varepsilon) \ln(1 + 2\varepsilon) + (\frac{1}{2} - \varepsilon) \ln(1 - 2\varepsilon)$ and $\lceil y \rceil$ denotes the smallest integer that is no less than y .

Proposition 1 shows that the probability of an unwatermarked image achieving a match rate substantially exceed-

ing $\frac{1}{2}$ decreases exponentially with the number of patches N . Hence, one can set the detection threshold slightly above $\frac{1}{2}$, and the false positive rate, i.e., the probability of misclassifying an unwatermarked image as a watermarked one, can be controlled with statistical guarantees. The proof is provided in Appendix A.

In practice, for the detection threshold, since $m(\mathbf{x}, \mathcal{W})$ follows a binomial distribution $B(N, \frac{1}{2})$, we can directly compute the threshold T_{match} for a target false positive rate fpr (e.g. 1%). Specifically, each candidate threshold $\frac{k}{N}$ has an associated **p-value**, which is the probability that a natural image achieves a match rate of at least $\frac{k}{N}$ under the binomial distribution. To find the threshold corresponding to the desired fpr , we iterate through candidate thresholds from $k = 0$ to $k = N$, compute the corresponding p-value for each, and select the first threshold whose associated p-value is at most fpr . The full procedure is summarized in Algorithm 1. With a properly calibrated T_{match} , the final detection process for a query image \mathbf{x} becomes straightforward. As described in Algorithm 2, we first compute its match rate $m(\mathbf{x}, \mathcal{W})$. If this value exceeds T_{match} , the image is classified as watermarked; otherwise, it is deemed unwatermarked.

Algorithm 1 Setting Match Rate Threshold

Input: A pre-defined watermark $\mathcal{W} = (\mathbf{c}, \tau)$ with N patches; A desired false positive rate fpr .

Output: The match rate threshold T_{match} .

```

1: for  $k = 0, \dots, N$  do
2:    $p_k \leftarrow \frac{1}{2^N} \sum_{i=k}^N \binom{N}{i}$        $\triangleright$  Tail prob. of  $B(N, \frac{1}{2})$ 
3:   if  $p_k \leq fpr$  then
4:      $T_{match} \leftarrow k/N$ 
5:     break
6:   end if
7: end for
8: return  $T_{match}$ 

```

Algorithm 2 Certified Watermark Detection

Input: An query image \mathbf{x} ; A watermark $\mathcal{W} = (\mathbf{c}, \tau)$, a match rate threshold T_{match} .

Output: Detection decision (Boolean)

```

1: Let  $\{\mathbf{p}_1, \dots, \mathbf{p}_N\}$  be the patches of  $\mathbf{x}$ .
2:  $m \leftarrow \frac{1}{N} \sum_{i=1}^N \mathbb{I}[\text{sgn}(l(\mathbf{p}_i) - \tau_i) = c_i]$ 
3: return ( $m \geq T_{match}$ )

```

3.3. Watermark Injection via Step-wise Guidance

Originally proposed in the diffusion model literature, guidance (Dhariwal & Nichol, 2021; Ho & Salimans, 2022) has since become widely adopted in vision generation. For context, consider a diffusion model $D(\mathbf{x}_t, \sigma_t)$ trained to pro-

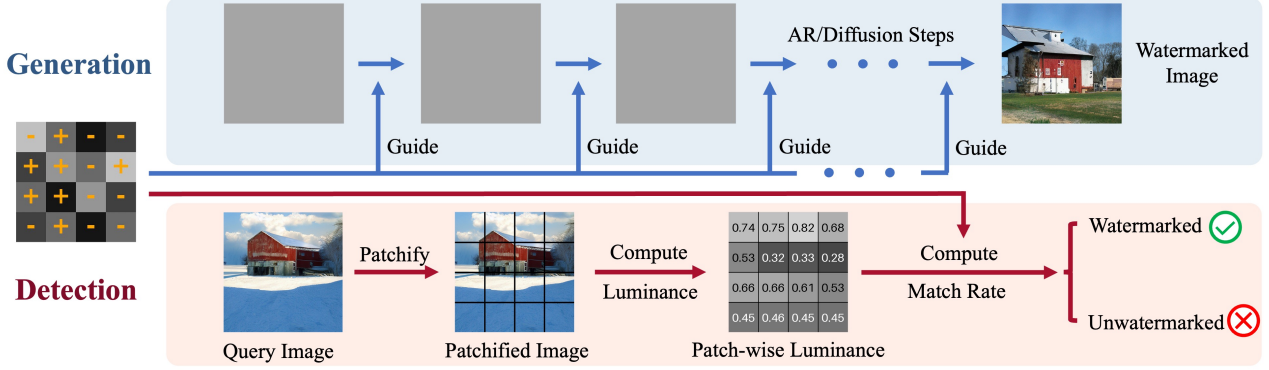


Figure 2. Illustration of Luminark. The watermark is defined as a patch-wise binary pattern (visualized by '+'/-' symbols) over the luminance values, i.e., whether the luminance exceeds the threshold (visualized by the grayscale intensity). Generation is performed by injecting the pattern using guidance. Detection is performed by comparing the pattern in the image and the predefined pattern.

gressively denoise a noisy input \mathbf{x}_t at time t . The sampling process is then a deterministic step-by-step denoising procedure that transforms Gaussian noise into a clean image, which can often be described by an ordinary differential equation (ODE) (Song et al., 2020b; Karras et al., 2022): $\frac{d\mathbf{x}_t}{dt} = \frac{\mathbf{x}_t - D(\mathbf{x}_t, \sigma_t)}{\sigma_t}$, $\mathbf{x}_T \sim \mathcal{N}(0, \sigma_{\max}^2 \mathbf{I})$, where σ_{\max} is the initial noise level at the start of the sampling process. In practice, this continuous process is approximated by numerical solvers such as the Euler method or Runge-Kutta methods (Süli & Mayers, 2003). Using the Euler method as an illustration, the generation process can be written as

$$\mathbf{x}_{t-1} = \mathbf{x}_t - \underbrace{\frac{\mathbf{x}_t - D(\mathbf{x}_t, \sigma_t)}{\sigma_t}}_{\text{Denoising Term}} (\sigma_t - \sigma_{t-1}), \quad t = T, \dots, 1 \quad (5)$$

Guidance techniques introduce additional modifications into Eqn.(4) to improve the quality of the generated images at each sampling step. For example, Classifier Guidance(CG) (Dhariwal & Nichol, 2021) modifies the update direction using an image classifier $p(y|\mathbf{x}_t)$:

$$\mathbf{x}_{t-1}^{CG} = \mathbf{x}_t^{CG} - \left[\underbrace{\frac{\mathbf{x}_t^{CG} - D(\mathbf{x}_t^{CG}, \sigma_t)}{\sigma_t} +}_{\text{Denoising Term}} \underbrace{s_t \nabla_{\mathbf{x}_t^{CG}} \log p(y|\mathbf{x}_t^{CG}; \sigma_t)}_{\text{Classifier Guidance Term}} \right] (\sigma_t - \sigma_{t-1}), \quad t = T, \dots, 1 \quad (6)$$

where s_t is a scale parameter that depends on the time t . Shortly thereafter, researchers generalized the concept of guidance beyond classifier-based targets. Notable extensions include Classifier-Free Guidance (Ho & Salimans, 2022) and Auto-Guidance (Karras et al., 2024a). More re-

cently, guidance has also been directly applied to other iterative generative frameworks, including autoregressive models (Tian et al., 2024) and autoregressive-diffusion hybrid models (Li et al., 2024), yielding significant performance gains.

We believe that guidance is well-suited to our scenario for two main reasons. First, prior studies have shown that guidance can be effectively applied across diverse generative paradigms, thereby satisfying the requirement for a general-purpose watermarking mechanism. Second, its inherent training-free nature makes guidance especially suitable for watermark injection: by defining a metric that quantifies the discrepancy between an intermediate generated image and the target watermark \mathcal{W} , the guidance process can progressively adjust the outcome in an adaptive manner.

Inspired by these works, we develop the Watermark Guidance(WG) to softly enforce the luminance constraints \mathcal{W} during generation. We first define an almost everywhere differentiable penalty function $\text{Penalty}(\mathbf{x}, \mathcal{W})$, serving as a surrogate of the match rate $m(\mathbf{x}, \mathcal{W})$ using a hinge-like loss:

$$\text{Penalty}(\mathbf{x}, \mathcal{W}) = \sum_{i=1}^N \max\{0, c_i \cdot (\tau_i - l(\mathbf{p}_i))\}. \quad (7)$$

The inner term $c_i \cdot (\tau_i - l(\mathbf{p}_i))$ is positive if and only if the constraint for patch i is violated, and the $\max\{0, \cdot\}$ operation ensures that satisfying all constraints contributes zero loss. We replace the original guidance term in Eqn.(5)

with this penalty and obtain the watermark-guided update:

$$\mathbf{x}_{t-1}^{\text{WG}} = \mathbf{x}_t^{\text{WG}} - \left[\underbrace{\frac{\mathbf{x}_t^{\text{WG}} - D(\mathbf{x}_t^{\text{WG}}, \sigma_t)}{\sigma_t}}_{\text{Denoising Term}} + \underbrace{s_t \nabla_{\mathbf{x}_t^{\text{WG}}} \text{Penalty}(\mathbf{x}_t^{\text{WG}}, \mathcal{W})}_{\text{Watermark Guidance Term}} \right] (\sigma_t - \sigma_{t-1}), \quad t = T, \dots, 1 \quad (8)$$

The full procedure is outlined in Algorithm 3. Above, we demonstrated our watermark guidance mechanism in the context of pixel-level diffusion models using the Euler method. One potential concern is the difficulty of extending our method to more complex settings. However, it is worth noting that in most recent models, guidance is typically formulated as additive terms within the step-wise update. To integrate our approach, we can simply either (a) apply watermark guidance to these models by replacing existing guidance terms, or (b) combine it with other additive guidance by simply appending the additional term. Appendix D and E provide detailed generation pipelines in representative models and the corresponding watermark injection implementations.

Algorithm 3 Luminark Injection via Guided Sampling

```

1: Input: Denoiser model  $D(\mathbf{x}, \sigma)$ , diffusion steps  $T$ , noise schedule  $\{\sigma_t\}_{t=0}^T$ , watermark  $\mathcal{W} = (\mathbf{c}, \tau)$ , watermark guidance scale  $s$ , threshold  $T$ 
2: repeat
3:   Initialize: sample  $\mathbf{x}_T \sim \mathcal{N}(0, \sigma_T^2 \mathbf{I})$ 
4:   for  $t = T, \dots, 1$  do
5:      $\mathbf{x}_{t-1} \leftarrow \mathbf{x}_t - \left[ \underbrace{\frac{\mathbf{x}_t - D(\mathbf{x}_t, \sigma_t)}{\sigma_t}}_{\text{Denoising}} + \underbrace{s \nabla_{\mathbf{x}_t} \text{Penalty}(\mathbf{x}_t, \mathcal{W})}_{\text{Guidance}} \right] (\sigma_t - \sigma_{t-1})$ 
6:   end for
7:    $m \leftarrow \sum_{i=1}^N \mathbb{I}[\text{sgn}(l(\mathbf{p}_i) - \tau_i) = c_i]$ 
8: until  $m \geq T$ 
9: return  $\mathbf{x}_0$ 

```

4. Experiment

For a comprehensive comparison, we conduct experiments on nine state-of-the-art ImageNet-pretrained generative

⁰To achieve successful injection, we repeatedly generate images until the match rate exceeds the threshold. In practice, the number of repetitions is typically small, e.g., about 2.3 in the EDM2 experiment.

models, as summarized in Table 2. These models span diverse architectures, parameter scales, and configurations. Building on this foundation, we adopt ImageNet as our primary experimental platform. Due to space limitations, the detailed baseline descriptions, hyperparameters, visualization, and extended results on the text-to-image scenario are provided in the appendix.

4.1. Robustness

Robustness aims to assess whether a watermark remains detectable after image transformations introduced by potential adversaries. In this subsection, we examine the robustness of our method against a range of practical image manipulations and compare its performance with baseline approaches.

We compare Luminark against four certified methods: classical approaches DwtDct (Cox et al., 1997), DwtDctSvd (Cox et al., 1997), and modern watermarking approaches in Tree-Ring family: Gaussian-Shading (GS) (Yang et al., 2024) and PRC-W (Gunn et al., 2024). The DwtDct and DwtDctSvd baselines are evaluated across all models, whereas the latter two are diffusion-specific, so we evaluate them only on EDMs. For all baselines, we use the official implementation if provided ¹. For our approach, the hyperparameters (e.g., patch size and watermark guidance scale) is provided in Appendix G. For each experiment, we first draw a unique watermark for each method and keep it fixed. Then, for every method, we sample 1,000 unwatermarked and 1,000 watermarked images. To assess robustness, each image is further subjected to nine different transformations: Scaling, Cropping, JPEG Compression, Filtering, Smoothing, Color Jitter, Color Quantization, Gaussian Noise, and Sharpening. The implementation for each transformation is detailed in Appendix B. We then re-apply watermark detection for each method on the transformed images and measure the detection accuracy. Each experiment is repeated 20 times with different random seeds to test the influence of watermark patterns and the sampled images. The average performance is reported.

Experimental Results. The experimental results are reported in Table 1. It can be seen that in all settings, our method consistently achieves accuracies of at least $\geq 95\%$, highlighting its wide applicability across different generative paradigms and reliable detectability under diverse transformations. Relative to prior methods, Luminark significantly outperforms post-hoc baselines (DwtDct $\sim 58\%$, DwtDctSvd $\sim 65\%$, RivaGAN $\sim 82\%$). Even when com-

¹Since Tian et al. (2024) did not release the inference code for VAR, we re-implemented it ourselves. The results reported here are based on our reproduction, which differs slightly from the original paper. We refer to MAR (Li et al., 2024) as a hybrid as it uses autoregressive generation with diffusion heads. For completeness, we describe Gaussian-Shading and PRC-W in detail in Appendix F.

Table 1. Detection accuracy under various image transformations. Luminark exhibits consistent robustness and performs competitively against strong baselines across all models and all attack types. Values exceeding 95% are highlighted in blue.

Model	Method	Scaling	Cropping	JPEG Comp.	Filtering	Smoothing	Color Jitter	Color Quant.	Gauss. Noise	Sharpening	Average
EDM2-XS	DwtDct	49.90	53.55	49.50	49.50	49.50	96.40	82.60	49.50	50.75	58.47
	DwtDctSvd	63.90	95.30	55.40	57.80	59.25	86.90	63.35	50.00	56.15	65.34
	GS.	99.51	99.50	99.52	99.50	99.50	99.49	99.48	99.50	99.49	99.50
	PRC-W.	94.00	99.40	98.35	93.05	97.20	99.50	98.40	91.75	99.40	96.79
	Ours	94.75	95.35	99.00	96.45	98.15	95.00	95.25	96.15	95.75	96.21
EDM2-L	DwtDct	49.90	53.60	49.50	49.50	49.50	96.60	82.25	49.50	50.75	58.51
	DwtDctSvd	63.45	95.60	55.20	57.60	59.50	86.00	63.45	50.00	56.25	65.23
	GS.	99.51	99.49	99.48	99.50	99.51	99.50	99.50	99.49	99.50	99.50
	PRC-W.	92.80	99.35	98.10	90.80	96.60	99.50	97.90	88.20	99.45	95.86
	Ours	94.65	95.15	98.60	96.15	98.00	94.65	95.15	96.00	96.00	95.49
EDM2-XXL	DwtDct	49.90	53.60	49.50	49.50	49.50	95.95	82.00	49.50	50.75	58.36
	DwtDctSvd	63.65	96.05	55.30	57.65	59.30	86.65	63.35	50.00	56.15	65.34
	GS.	99.51	99.50	99.48	99.50	99.50	99.49	99.50	99.50	99.50	99.50
	PRC-W.	98.00	99.50	98.60	95.70	98.90	99.50	98.35	89.00	99.35	97.44
	Ours	95.50	96.00	99.20	96.60	98.35	94.50	95.40	95.90	95.65	95.23
VAR-d16	DwtDct	49.90	53.60	49.50	49.50	49.50	95.50	82.10	49.50	50.75	58.31
	DwtDctSvd	63.75	95.80	55.25	57.75	59.45	87.05	63.35	50.00	56.05	65.39
	Ours	96.00	95.65	98.85	96.70	97.85	95.30	94.50	96.10	96.40	95.81
VAR-d30	DwtDct	49.90	53.65	49.50	49.50	49.50	96.75	82.15	49.50	50.75	58.47
	DwtDctSvd	63.50	95.55	55.30	57.50	59.30	86.95	63.55	50.00	56.10	65.31
	Ours	96.00	96.15	98.90	96.80	98.60	95.95	95.45	95.90	95.35	96.01
VAR-d36	DwtDct	49.90	53.60	49.50	49.50	49.50	96.80	81.85	49.50	50.75	58.44
	DwtDctSvd	63.65	95.65	55.30	57.80	59.20	86.45	63.10	50.00	56.20	65.26
	Ours	96.30	96.25	98.90	96.05	97.90	94.50	95.75	96.40	96.50	95.95
MAR-Base	DwtDct	49.90	53.65	49.50	49.50	49.50	96.65	81.45	49.50	50.75	58.38
	DwtDctSvd	63.45	95.55	55.35	57.75	59.35	87.35	63.40	50.00	56.20	65.38
	Ours	95.90	96.75	99.50	97.15	97.55	94.95	95.00	95.90	96.30	96.56
MAR-Large	DwtDct	49.90	53.60	49.50	49.50	49.50	96.20	82.35	49.50	50.75	58.42
	DwtDctSvd	63.60	95.20	55.35	57.55	59.25	86.30	63.15	50.00	56.15	65.17
	Ours	95.85	95.35	99.50	97.00	98.70	94.85	94.75	95.25	95.85	95.79
MAR-Huge	DwtDct	49.90	53.55	49.50	49.50	49.50	96.80	82.65	49.50	50.75	58.52
	DwtDctSvd	63.40	95.35	55.30	57.75	59.30	86.00	63.45	50.00	56.20	65.19
	Ours	94.75	95.10	99.15	96.30	98.55	95.35	94.80	96.65	96.50	95.80

Table 2. Generation quality of watermarked images using different methods. Ref. denotes the FID of unwatermarked images generated by each model. Luminark clearly outperforms previous methods, achieving FID scores that closely approach the Ref. values.

Model	Paradigm	Tokenizer	Resolution	Param.	FID↓				
					GS.	PRC-W.	Ours	Ref.	
EDM2-XS	Diffusion	Continuous	512×512	0.25 B	6.99	6.88	4.40	3.53	
EDM2-L	Diffusion	Continuous	512×512	1.56 B	5.08	5.00	2.72	2.06	
EDM2-XXL	Diffusion	Continuous	512×512	3.05 B	4.87	4.60	2.13	1.81	
VAR-d16	AR.	Discrete	256×256	0.31 B	Not Applicable		4.04	3.47	
VAR-d30	AR.	Discrete	256×256	2.01 B	Not Applicable		3.06	2.05	
VAR-d36	AR.	Discrete	512×512	2.35 B	Not Applicable		4.22	2.76	
MAR-Base	Hybrid	Continuous	256×256	0.21 B	Not Applicable		3.88	2.31	
MAR-Large	Hybrid	Continuous	256×256	0.48 B	Not Applicable		3.32	1.78	
MAR-Huge	Hybrid	Continuous	256×256	0.94 B	Not Applicable		3.09	1.55	

pared with diffusion-specific approaches on EDMs, Luminark remains highly competitive: its average performance is nearly the same as PRC-W and only marginally below Gaussian-Shading. We attribute the success of Luminark to its use of a regional statistical signature that is inherently more robust—while individual pixel values may vary, the patch-wise statistical properties are largely preserved. Due to space limitations, we cannot test all possible transforma-

tions. A natural concern is that certain common operations, such as flipping, could lead to huge detection mistakes. This issue can be addressed with a straightforward strategy: for any given image, we apply the watermark detector to both the original and its flipped version, and then use the logical “OR” of the two outcomes as the final detection result.

4.2. Fidelity

Following standard practice, we use the Fréchet Inception Distance (FID) (Heusel et al., 2017) to evaluate the generation quality of image generative models. We conduct experiments on the same set of models as in Section 4.1 and compare Luminark with Gaussian-Shading and PRC-W. The three post-hoc baselines are excluded from this evaluation due to their weak robustness. For each experiment, we first sample a unique watermark for each method and keep it fixed. Then, for each method, we generate 50,000 watermarked images and compute the FID scores against the clean image dataset. Each experiment is repeated 20 times, and the average performance is reported.

Experimental Results. As shown in Table 2, the FID scores of watermarked images with Luminark significantly surpass those of Gaussian-Shading and PRC-W, while closely approaching the non-watermarked references across all nine models. The differences between Luminark and the reference values are generally around 1.0. Notably, the FID of watermarked EDM2-XXL is only 2.13, demonstrating exceptionally high generation quality. In comparison, Gaussian-Shading and PRC-W nearly double the reference FID score, not to mention they are not applicable in VAR and MAR. We further extend the evaluation to Stable Diffusion v2.1, using MS-COCO validation set (30K samples). The FID and CLIP score are reported in Table 3.

In Appendix C, we present visualizations of watermarked and unwatermarked images generated by the nine models with the same seed as well as watermarked Stable Diffusion, revealing several interesting phenomena. First, in some cases (e.g., the first image in Figure 15), our guidance induces only subtle modifications, such as minor variations in brightness or texture, to satisfy the watermark. In other cases (e.g., the third image in Figure 14), the model introduces additional objects to meet the constraint. This demonstrates that the models have sufficient capacity to adaptively and even creatively adjust the content to embed the watermark and maintain generation quality simultaneously.

4.3. Ablation Study

Luminark makes two key contributions: a novel watermark pattern and a general injection algorithm. An important question is whether either component could be substituted by conventional methods, and how each individually con-

tributes to the overall success. In this subsection, we present ablation studies addressing this question and confirm that both components are essential.

Comparison I: Luminark’s watermark with other injection methods. We investigate whether watermark injection can be achieved through more straightforward approaches than guidance. To this end, we design two baseline methods: (i) post-hoc projection, which directly enforces a percentage of the luminance constraint only after the image has been fully generated; and (ii) hard step-wise projection, which forces a fixed percentage of patches to satisfy the constraint at every step of the generation process. We conduct our experiments on three representative models: EDM2-L, VAR-d30, and MAR-Large. As shown in Table 4, both post-hoc projection and hard step-wise injection significantly degrade image quality as they introduce obvious block artifacts. In contrast, our guidance method enables the model to adaptively balance the two objectives, yielding high-quality outputs.

Comparison II: Guided injection with other watermarks. We investigate whether guidance can be combined with other watermark patterns to achieve performance comparable to Luminark. It is immediately clear that post-hoc watermarks discussed previously are bound to fail as they are non-robust, and diffusion-specific watermarks are incompatible. Luminark employs a specific linear combination of RGB values to construct the watermark. An interesting question is whether alternative combinations would also be effective. To investigate this, we design five variants: using only the R channel, only the G channel, only the B channel, the RGB average, as well as a random linear combination. Experiments are conducted on EDM2-L, VAR-d30, and MAR-Large. As shown in Table 4, all alternatives lead to higher FID scores. This observation appears surprising, but can be partially understood from a perceptual perspective. Luminance has long been recognized as a dominant factor in image processing (Buchsbaum, 1980; Bovik, 2010; Simoncelli & Olshausen, 2001): principal component analyses consistently reveal that the first component of image data aligns closely with the perceptual notion of luminance. This intrinsic concentration of information in the luminance channel may explain why enforcing watermark constraints along this axis preserves generation quality more effectively than using arbitrary linear combinations of RGB values.

5. Conclusions, Limitations, and Future Directions

In this work, we presented Luminark, a reliable and general watermarking method for vision generative models. By introducing a novel watermark pattern based on patch-level luminance statistics, Luminark provides a reliable detection mechanism with a statistical guarantee. To enable practical

Table 4. Ablation study

Model	Luminark	With other watermark					With other injection method	
		R	G	B	Average	Random	Post-hoc	Hard Step-wise
EDM2-L	2.72	3.01	3.39	4.30	3.48	3.03	16.70	92.05
VAR-d30	3.06	3.08	3.26	3.74	3.32	3.52	7.68	33.25
MAR-L	3.32	3.50	3.49	4.89	3.41	4.06	6.88	85.15

and model-agnostic watermark injection, we leveraged the widely adopted guidance technique and extended it into a plug-and-play watermark guidance framework. Comprehensive experiments demonstrate the effectiveness of our approach. According to our experience, the current version of Luminark has two limitations that can be addressed with further research. (a). The first limitation lies in the computational cost of generation, including the repeated sampling and additional backpropagation steps. We believe this issue can be mitigated through the use of a more effective penalty function and careful optimization, such as employing sparse WG updates or adopting early stopping strategies for WG when sufficient alignment has been achieved. (b). Secondly, we believe there remains room for further improvement in generation quality, particularly for MAR models. Potential solutions include adopting more fine-grained watermark patterns, as well as exploring adaptive guidance strategies.

References

Arabi, K., Feuer, B., Witter, R. T., Hegde, C., and Cohen, N. Hidden in the noise: Two-stage robust watermarking for images. *arXiv preprint arXiv:2412.04653*, 2024.

Bi, N., Sun, Q., Huang, D., Yang, Z., and Huang, J. Robust image watermarking based on multiband wavelets and empirical mode decomposition. *IEEE Transactions on Image Processing*, 16(8):1956–1966, 2007.

Bovik, A. C. *Handbook of image and video processing*. Academic press, 2010.

Buchsbaum, G. A spatial processor model for object colour perception. *Journal of the Franklin institute*, 310(1):1–26, 1980.

Bui, T., Agarwal, S., and Collomosse, J. Trustmark: Universal watermarking for arbitrary resolution images. *arXiv preprint arXiv:2311.18297*, 2023.

Choi, H., Won, S., Hwang, D., and Choi, J. Readme: Robust error-aware digital signature framework via deep watermarking model. *arXiv preprint arXiv:2507.04495*, 2025.

Ci, H., Song, Y., Yang, P., Xie, J., and Shou, M. Z. Wmadapter: Adding watermark control to latent diffusion models. *arXiv preprint arXiv:2406.08337*, 2024a.

Ci, H., Yang, P., Song, Y., and Shou, M. Z. Ringid: Rethinking tree-ring watermarking for enhanced multi-key identification. In *European Conference on Computer Vision*, pp. 338–354. Springer, 2024b.

Cox, I., Miller, M., Bloom, J., Fridrich, J., and Kalker, T. *Digital Watermarking and Steganography*. Morgan Kaufmann Publishers Inc., San Francisco, CA, USA, 2 edition, 2007. ISBN 9780080555805.

Cox, I. J., Kilian, J., Leighton, F. T., and Shamoon, T. Secure spread spectrum watermarking for multimedia. *IEEE transactions on image processing*, 6(12):1673–1687, 1997.

Dhariwal, P. and Nichol, A. Diffusion models beat gans on image synthesis. *Advances in neural information processing systems*, 34:8780–8794, 2021.

Dosovitskiy, A., Beyer, L., Kolesnikov, A., Weissenborn, D., Zhai, X., Unterthiner, T., Dehghani, M., Minderer, M., Heigold, G., Gelly, S., et al. An image is worth 16x16 words: Transformers for image recognition at scale. *arXiv preprint arXiv:2010.11929*, 2020.

Evennou, G., Chappelier, V., and Kijak, E. Fast, secure, and high-capacity image watermarking with autoencoded text vectors. *arXiv preprint arXiv:2510.00799*, 2025.

Fairoze, J., Ortiz-Jimenez, G., Vecerik, M., Jha, S., and Gowal, S. On the difficulty of constructing a robust and publicly-detectable watermark. *arXiv preprint arXiv:2502.04901*, 2025.

Fares, S., Tastan, N., and Nandakumar, K. Spdmark: Selective parameter displacement for robust video watermarking. *arXiv preprint arXiv:2512.12090*, 2025.

Fernandez, P., Couairon, G., Jégou, H., Douze, M., and Furon, T. The stable signature: Rooting watermarks in latent diffusion models. In *Proceedings of the IEEE/CVF International Conference on Computer Vision*, pp. 22466–22477, 2023.

Gesny, E., Giboulot, E., Furon, T., and Chappelier, V. Guidance watermarking for diffusion models. *arXiv preprint arXiv:2509.22126*, 2025.

Gonzalez, R. C. and Woods, R. E. *Digital Image Processing*. Pearson, 4th edition, 2018.

Gowal, S., Bunel, R., Stimberg, F., Stutz, D., Ortiz-Jimenez, G., Kouridi, C., Vecerik, M., Hayes, J., Rebuffi, S.-A., Bernard, P., et al. Synthid-image: Image watermarking at internet scale. *arXiv preprint arXiv:2510.09263*, 2025.

Gunn, S., Zhao, X., and Song, D. An undetectable watermark for generative image models. *arXiv preprint arXiv:2410.07369*, 2024.

Heusel, M., Ramsauer, H., Unterthiner, T., Nessler, B., and Hochreiter, S. Gans trained by a two time-scale update rule converge to a local nash equilibrium. *Advances in neural information processing systems*, 30, 2017.

Ho, J. and Salimans, T. Classifier-free diffusion guidance. *arXiv preprint arXiv:2207.12598*, 2022.

Ho, J., Jain, A., and Abbeel, P. Denoising diffusion probabilistic models. *Advances in neural information processing systems*, 33:6840–6851, 2020.

Hoeffding, W. Probability inequalities for sums of bounded random variables. *Journal of the American statistical association*, 58(301):13–30, 1963.

Hsieh, M.-S., Tseng, D.-C., and Huang, Y.-H. Hiding digital watermarks using multiresolution wavelet transform. *IEEE Transactions on industrial electronics*, 48(5):875–882, 2001.

Huang, H., Wu, Y., and Wang, Q. Robin: Robust and invisible watermarks for diffusion models with adversarial optimization. *Advances in Neural Information Processing Systems*, 37:3937–3963, 2024.

Huang, Y., Chen, J., Zheng, Q., Li, H., Liu, S., and Hu, X. Video signature: In-generation watermarking for latent video diffusion models. *arXiv preprint arXiv:2506.00652*, 2025.

Jovanović, N., Labiad, I., Souček, T., Vechev, M., and Fernandez, P. Watermarking autoregressive image generation. *arXiv preprint arXiv:2506.16349*, 2025.

Karras, T., Aittala, M., Aila, T., and Laine, S. Elucidating the design space of diffusion-based generative models. *Advances in neural information processing systems*, 35: 26565–26577, 2022.

Karras, T., Aittala, M., Kynkänniemi, T., Lehtinen, J., Aila, T., and Laine, S. Guiding a diffusion model with a bad version of itself. *Advances in Neural Information Processing Systems*, 37:52996–53021, 2024a.

Karras, T., Aittala, M., Lehtinen, J., Hellsten, J., Aila, T., and Laine, S. Analyzing and improving the training dynamics of diffusion models. In *Proceedings of the IEEE/CVF Conference on Computer Vision and Pattern Recognition*, pp. 24174–24184, 2024b.

Kerner, L., Meintz, M., Zhao, B., Boenisch, F., and Dziedzic, A. Bitmark for infinity: Watermarking bitwise autoregressive image generative models. *arXiv preprint arXiv:2506.21209*, 2025.

Lee, S. J. and Cho, N. I. Semantic watermarking reinvented: Enhancing robustness and generation quality with fourier integrity. In *Proceedings of the IEEE/CVF International Conference on Computer Vision*, pp. 18759–18769, 2025.

Li, T., Tian, Y., Li, H., Deng, M., and He, K. Autoregressive image generation without vector quantization. *Advances in Neural Information Processing Systems*, 37:56424–56445, 2024.

Lipman, Y., Chen, R. T., Ben-Hamu, H., Nickel, M., and Le, M. Flow matching for generative modeling. *arXiv preprint arXiv:2210.02747*, 2022.

Lu, S., Zhou, Z., Lu, J., Zhu, Y., and Kong, A. W.-K. Robust watermarking using generative priors against image editing: From benchmarking to advances. *arXiv preprint arXiv:2410.18775*, 2024.

Mao, P.-Y., Tsai, C.-C., and Lu, C.-S. Maxsive: High-capacity and robust training-free generative image watermarking in diffusion models. In *Proceedings of the 33rd ACM International Conference on Multimedia*, pp. 11443–11452, 2025.

Min, R., Li, S., Chen, H., and Cheng, M. A watermark-conditioned diffusion model for ip protection. In *European Conference on Computer Vision*, pp. 104–120. Springer, 2024.

Pereira, S. and Pun, T. Robust template matching for affine resistant image watermarks. *IEEE transactions on image Processing*, 9(6):1123–1129, 2000.

Potdar, V. M., Han, S., and Chang, E. A survey of digital image watermarking techniques. In *INDIN'05. 2005 3rd IEEE International Conference on Industrial Informatics*, 2005., pp. 709–716. IEEE, 2005.

Radford, A., Wu, J., Child, R., Luan, D., Amodei, D., Sutskever, I., et al. Language models are unsupervised multitask learners. *OpenAI blog*, 1(8):9, 2019.

Rombach, R., Blattmann, A., Lorenz, D., Esser, P., and Ommer, B. High-resolution image synthesis with latent diffusion models, 2021.

Rombach, R., Blattmann, A., Lorenz, D., Esser, P., and Ommer, B. High-resolution image synthesis with latent diffusion models. In *Proceedings of the IEEE/CVF conference on computer vision and pattern recognition*, pp. 10684–10695, 2022.

Sander, T., Fernandez, P., Durmus, A., Furou, T., and Douze, M. Watermark anything with localized messages. *arXiv preprint arXiv:2411.07231*, 2024.

Simoncelli, E. P. and Olshausen, B. A. Natural image statistics and neural representation. *Annual review of neuroscience*, 24(1):1193–1216, 2001.

Song, J., Meng, C., and Ermon, S. Denoising diffusion implicit models. *arXiv preprint arXiv:2010.02502*, 2020a.

Song, Y., Sohl-Dickstein, J., Kingma, D. P., Kumar, A., Ermon, S., and Poole, B. Score-based generative modeling through stochastic differential equations. *arXiv preprint arXiv:2011.13456*, 2020b.

Song, Y., Dhariwal, P., Chen, M., and Sutskever, I. Consistency models. 2023.

Souček, T., Fernandez, P., Elsahar, H., Rebuffi, S.-A., Lactatu, V., Tran, T., Sander, T., and Mourachko, A. Pixel seal: Adversarial-only training for invisible image and video watermarking. *arXiv preprint arXiv:2512.16874*, 2025.

Süli, E. and Mayers, D. F. *An introduction to numerical analysis*. Cambridge university press, 2003.

Szeliski, R. *Computer Vision: Algorithms and Applications*. Springer, 2022.

Tian, K., Jiang, Y., Yuan, Z., Peng, B., and Wang, L. Visual autoregressive modeling: Scalable image generation via next-scale prediction. *Advances in neural information processing systems*, 37:84839–84865, 2024.

Vaswani, A., Shazeer, N., Parmar, N., Uszkoreit, J., Jones, L., Gomez, A. N., Kaiser, Ł., and Polosukhin, I. Attention is all you need. *Advances in neural information processing systems*, 30, 2017.

Wang, Z., Guo, J., Zhu, J., Li, Y., Huang, H., Chen, M., and Tu, Z. Sleepermark: Towards robust watermark against fine-tuning text-to-image diffusion models. In *Proceedings of the Computer Vision and Pattern Recognition Conference*, pp. 8213–8224, 2025.

Wen, Y., Kirchenbauer, J., Geiping, J., and Goldstein, T. Tree-ring watermarks: Fingerprints for diffusion images that are invisible and robust. *arXiv preprint arXiv:2305.20030*, 2023.

Yang, J., Fang, H., Zhang, W., Yu, N., and Chen, K. T2smark: Balancing robustness and diversity in noise-as-watermark for diffusion models. *arXiv preprint arXiv:2510.22366*, 2025.

Yang, Z., Zeng, K., Chen, K., Fang, H., Zhang, W., and Yu, N. Gaussian shading: Provable performance-lossless image watermarking for diffusion models. In *Proceedings of the IEEE/CVF Conference on Computer Vision and Pattern Recognition*, pp. 12162–12171, 2024.

Zhang, G., Wang, L., Su, Y., and Liu, A.-A. Markplunger: Generalizable watermark framework for latent diffusion models without retraining. *IEEE Transactions on Multimedia*, 2025.

Zhang, L., Liu, X., Martin, A. V., Bearfield, C. X., Brun, Y., and Guan, H. Robust image watermarking using stable diffusion. *arXiv preprint arXiv:2401.04247*, 2024.

Zhao, Y., Pang, T., Du, C., Yang, X., Cheung, N.-M., and Lin, M. A recipe for watermarking diffusion models. *arXiv preprint arXiv:2303.10137*, 2023.

A. Proof of Proposition 1

Proof. We introduce the auxiliary random variables $Z_i = \mathbb{I}[\text{sgn}(l(\mathbf{p}_i) - \tau_i) = c_i]$, $i = 1, \dots, N$, so that $m(\mathbf{x}, \mathcal{W}) = \frac{1}{N} \sum_{i=1}^N Z_i$. We first show that the variables $\{Z_i\}_{i=1}^N$ are i.i.d and each follows a Bernoulli($\frac{1}{2}$) distribution with support $\{0, 1\}$. The independence follows directly from the fact that the variables $\{c_i\}_{i=1}^N$ are independently sampled. It is evident that the support of Z_i is $\{0, 1\}$, then we have $\Pr(Z_i = 1) = \Pr(c_i = \text{sgn}(l(\mathbf{p}_i) - \tau_i)) = \Pr(l(\mathbf{p}_i) \geq \tau_i) \Pr(c_i = 1) + \Pr(l(\mathbf{p}_i) < \tau_i) \Pr(c_i = -1) = \frac{1}{2}l(\mathbf{p}_i) + \frac{1}{2}(1 - l(\mathbf{p}_i)) = \frac{1}{2}$. Then we further have $\Pr(Z_i = 0) = \frac{1}{2}$, and the theorem yields by directly applying the Chernoff–Hoeffding theorem (Hoeffding, 1963). \square

B. Implementation of Image Transformations for Robust Detection

This appendix provides the Python code snippets used for the image manipulation attacks in our robustness evaluation. Each function takes a watermarked image as a NumPy array (in BGR channel order, as used by OpenCV) and returns the transformed image. The specific parameters used in our experiments are hardcoded in these functions for clarity and reproducibility.

Scaling

```
def scaling_attack(image: np.ndarray) -> np.ndarray:
    """Downscales to 96x96, then scales back to original size."""
    original_size = (image.shape[1], image.shape[0])
    downscaled = cv2.resize(image, (96, 96), interpolation=cv2.INTER_LINEAR)
    restored = cv2.resize(downscaled, original_size,
                          interpolation=cv2.INTER_LINEAR)
    return restored
```

Cropping

```
def cropping_attack(image: np.ndarray) -> np.ndarray:
    """Crops a 2-pixel border and resizes back to original."""
    original_size = (image.shape[1], image.shape[0])
    # For a 512x512 image, this crops to a 510x510 region from (2,2)
    cropped = image[2:-2, 2:-2]
    restored = cv2.resize(cropped, original_size, interpolation=cv2.INTER_LINEAR)
    return restored
```

JPEG Compression

```
def jpeg_compression_attack(image: np.ndarray) -> np.ndarray:
    """Applies JPEG compression with a quality factor of 50."""
    pil_image = Image.fromarray(cv2.cvtColor(image, cv2.COLOR_BGR2RGB))
    buffer = io.BytesIO()
    pil_image.save(buffer, format='JPEG', quality=50)
    buffer.seek(0)
    compressed_pil = Image.open(buffer)
    compressed_cv = cv2.cvtColor(np.array(compressed_pil), cv2.COLOR_RGB2BGR)
    return compressed_cv
```

Filtering (Median)

```
def filtering_attack(image: np.ndarray) -> np.ndarray:
    """Applies a median filter with an 11x11 kernel."""
    return cv2.medianBlur(image, 11)
```

Smoothing (Gaussian Blur)

```
def smoothing_attack(image: np.ndarray) -> np.ndarray:
    """Applies a Gaussian blur with a 9x9 kernel and sigma=15."""
    return cv2.GaussianBlur(image, (9, 9), 15)
```

Color Jitter

```
def color_jitter_attack(image: np.ndarray) -> np.ndarray:
    """Applies random color jitter with a factor of 0.1."""
    # Brightness, Saturation, Hue jitter in HSV space
    hsv = cv2.cvtColor(image, cv2.COLOR_BGR2HSV).astype(np.float32)
    hsv[:, :, 0] *= (1 + random.uniform(-0.1, 0.1)) # Hue
    hsv[:, :, 1] *= (1 + random.uniform(-0.1, 0.1)) # Saturation
    hsv[:, :, 2] *= (1 + random.uniform(-0.1, 0.1)) # Brightness
    np.clip(hsv[:, :, 0], 0, 179, out=hsv[:, :, 0])
    np.clip(hsv[:, :, 1:], 0, 255, out=hsv[:, :, 1:])
    jittered = cv2.cvtColor(hsv.astype(np.uint8), cv2.COLOR_HSV2BGR)

    # Contrast jitter using Pillow
    pil_img = Image.fromarray(cv2.cvtColor(jittered, cv2.COLOR_BGR2RGB))
    enhancer = ImageEnhance.Contrast(pil_img)
    contrast_factor = 1 + random.uniform(-0.1, 0.1)
    final_image = enhancer.enhance(contrast_factor)

    return cv2.cvtColor(np.array(final_image), cv2.COLOR_RGB2BGR)
```

Color Quantization

```
def color_quantization_attack(image: np.ndarray) -> np.ndarray:
    """Reduces the number of colors to 64 using k-means in CIELAB space."""
    lab_image = cv2.cvtColor(image, cv2.COLOR_BGR2LAB)
    pixel_data = np.float32(lab_image.reshape((-1, 3)))
    criteria = (cv2.TERM_CRITERIA_EPS + cv2.TERM_CRITERIA_MAX_ITER, 20, 1.0)
    _, labels, centers = cv2.kmeans(pixel_data, 64, None, criteria, 10,
                                    cv2.KMEANS_RANDOM_CENTERS)
    centers = np.uint8(centers)
    quantized_lab = centers[labels.flatten()].reshape(lab_image.shape)
    return cv2.cvtColor(quantized_lab, cv2.COLOR_LAB2BGR)
```

Gaussian Noise

```
def gaussian_noise_attack(image: np.ndarray) -> np.ndarray:
    """Adds Gaussian noise with mean=0 and std=25."""
    noise = np.random.normal(0, 25, image.shape)
    noisy_image = np.clip(image.astype(np.float32) + noise, 0, 255)
    return noisy_image.astype(np.uint8)
```

Sharpening

```
def sharpening_attack(image: np.ndarray) -> np.ndarray:
    """Applies an Unsharp Mask filter with radius=5 and strength=300%."""
    pil_image = Image.fromarray(cv2.cvtColor(image, cv2.COLOR_BGR2RGB))
    # 'percent' controls strength, 'threshold' is left at default
    sharpened = pil_image.filter(ImageFilter.UnsharpMask(radius=5, percent=300))
    return cv2.cvtColor(np.array(sharpened), cv2.COLOR_RGB2BGR)
```

C. Visualization of the Watermarked Images

For all the figures in this section, $\mathcal{W} = (\mathbf{c}, \tau)$ is fixed within each experiment. Images generated by the vanilla pipeline are placed at the top, watermarked images with Luminark using the same seeds are placed in the middle, and visualization of $\mathcal{W} = (\mathbf{c}, \tau)$ are placed at the bottom. In the bottom row, each cell corresponds to a patch: grayscale intensity encodes τ (lighter = larger luminance); $+$ / $-$ symbols denote \mathbf{c} ; symbol color indicates whether the luminance constraint is satisfied (green) or violated (red) in the corresponding watermarked image. Since Stable Diffusion is a diffusion-based model, it is naturally compatible with guidance. We directly extend our approach to the text-to-image scenario.



Figure 3. Visualization of Stable-Diffusion Version2.1: Prompt (left): The Gates of Valhalla, grand and imposing, with Valkyries flying around, Norse mythology, epic, divine lighting, matte painting, masterpiece. Prompt (mid): A cheerful anime girl with vibrant pink hair and large expressive eyes, wearing a school uniform, cherry blossoms falling, digital art, by Makoto Shinkai. Prompt (right): A stoic Roman centurion in full armor, standing guard, detailed armor and helmet, realistic, cinematic shot.



Figure 4. Visualization of Stable-Diffusion Version2.1 Prompt (left): A field of glowing lavender under the Milky Way, astrophotography, stunning, magical, long exposure. Prompt (mid): A quaint, cobblestone alleyway in a European village, colorful houses with flower boxes, charming, sunny day. Prompt (right): A luxurious Art Deco hotel lobby, geometric patterns, gold and black color scheme, elegant, 1920s style.



Figure 5. Visualization of Stable-Diffusion Version2.1: Prompt (left): An infinity pool on a rooftop overlooking a modern city skyline at dusk, luxurious, serene, beautiful view. Prompt (mid): The interior of a futuristic spaceship bridge, holographic displays, panoramic view of space, clean design, sci-fi. Prompt (right): An ancient, ruined Greek temple on a cliffside, overlooking the Aegean Sea, historical, majestic, golden hour.

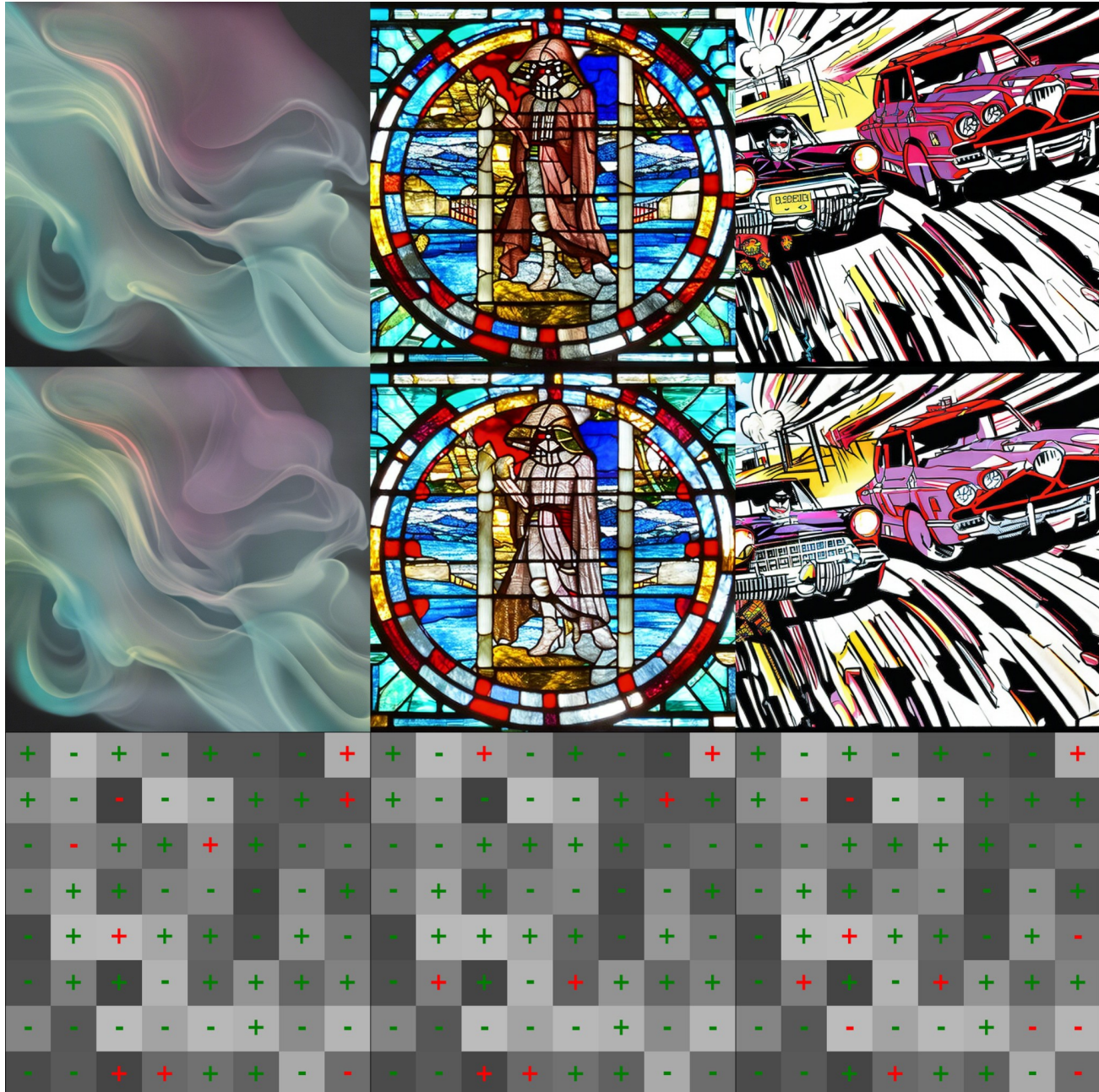


Figure 6. Visualization of Stable-Diffusion Version2.1: Prompt (left): "Serenity" visualized as flowing, pastel-colored liquid smoke, on a dark background, abstract art, calming, high resolution. Prompt (mid): A stained glass window depicting a scene from Star Wars, intricate, colorful, beautiful. Prompt (right): A car chase scene in a comic book art style, dynamic action lines, bold colors, halftone patterns, by Jack Kirby.



Figure 7. Visualization of Stable-Diffusion Version2.1 Prompt (left): A pair of worn-out hiking boots, covered in mud, resting on a wooden porch after a long journey, telling a story. Prompt (mid): An artist’s messy studio, canvases, paint tubes, brushes scattered everywhere, creative chaos, natural light from a large window. Prompt (right): A squirrel curiously peeking from behind a tree, soft background blur (bokeh), wildlife photography.

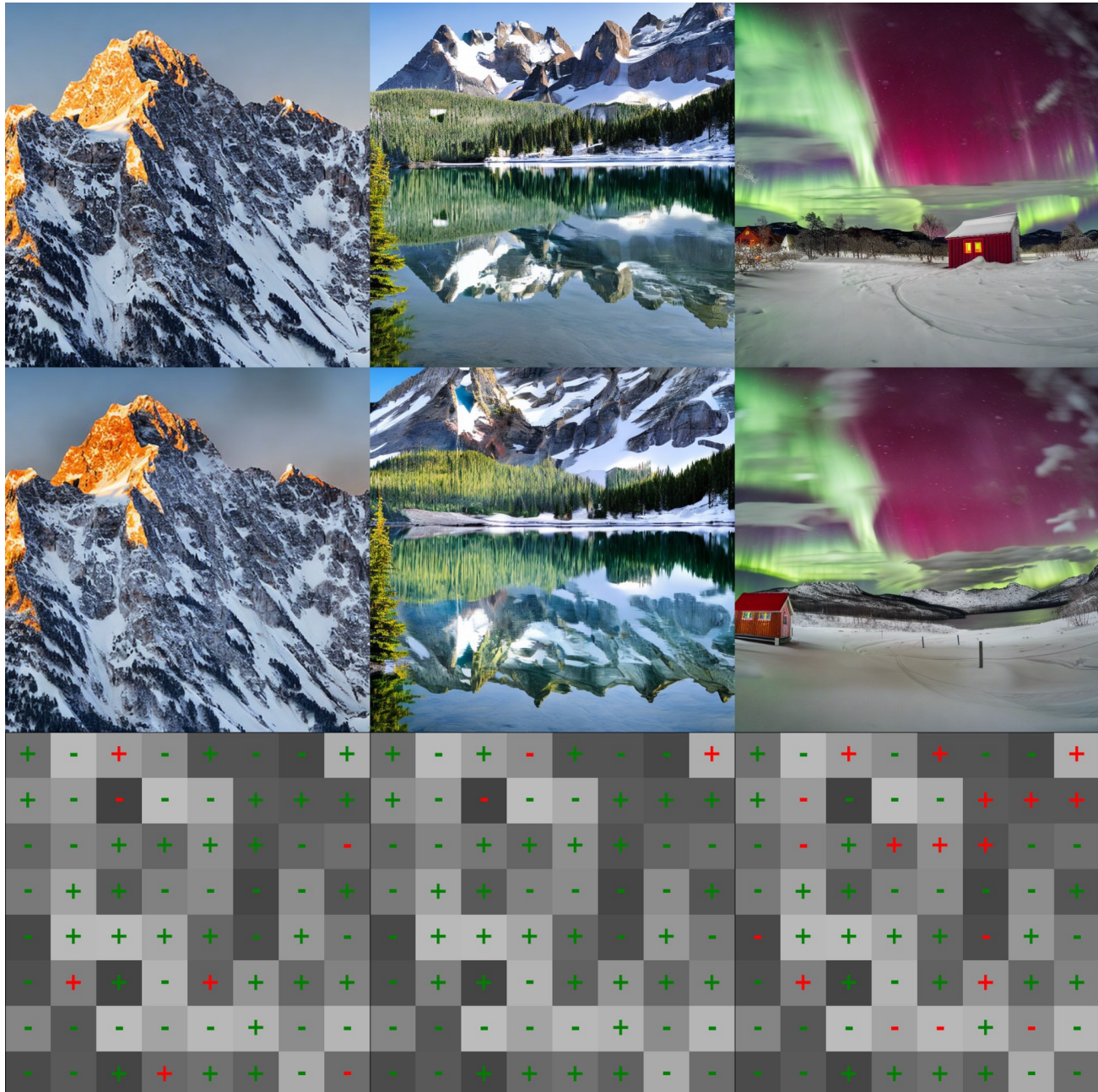


Figure 8. Visualization of Stable-Diffusion Version2.1: Prompt (left): Breathtaking panoramic photograph of the Swiss Alps at sunrise, golden light hitting the snow-capped peaks, f/16, wide-angle lens, professional landscape photography, 8k, hyper-detailed. Prompt (mid): A crystal-clear alpine lake in Canada, perfectly reflecting majestic, snow-dusted mountains, calm water, early morning light, professional landscape photo, sharp focus. Prompt (right): A vibrant aurora borealis (Northern Lights) dancing over a snow-covered landscape in Norway, with a small red cabin, professional night photography, shot with a wide-angle f/2.8 lens.

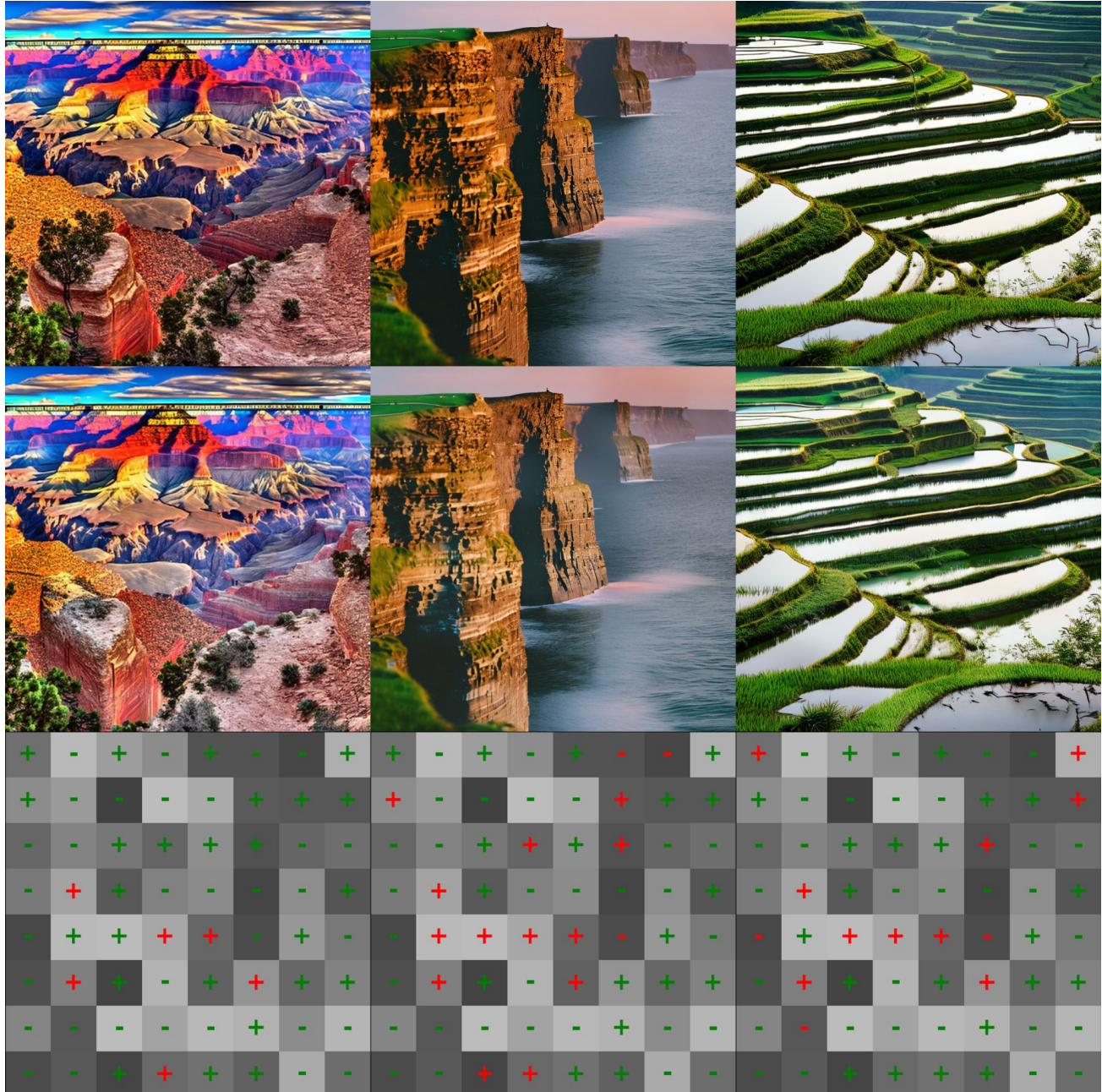


Figure 9. Visualization of Stable-Diffusion Version2.1: Prompt (left): The immense scale of the Grand Canyon at sunrise, layers of red and orange rock illuminated, epic panoramic view, high dynamic range (HDR) photo. Prompt (mid): Stunning sunset over the cliffs of Moher, Ireland, the sun dipping below the horizon casting a warm orange glow, shot on Kodak Portra 400 film, film grain, cinematic. Prompt (right): Rice terraces in Sapa, Vietnam, during the golden hour, beautiful layers and reflections in the water, lush green, professional travel photography.



Figure 10. Visualization of Stable-Diffusion Version2.1: Prompt (left): A charming coastal town in Santorini, Greece, iconic white buildings with blue domes overlooking the calm Aegean Sea, golden hour lighting, sharp details, travel magazine photo. Prompt (mid): The unique limestone karsts of Halong Bay, Vietnam, emerging from the emerald water, traditional junk boats sailing by, misty morning, atmospheric photo. Prompt (right): A close-up, wide-angle shot of a surreal black sand beach in Iceland, with chunks of glistening ice washed ashore like diamonds, soft morning light, intricate details.



Figure 11. Visualization of Stable-Diffusion Version2.1: Prompt (left): The Fairy Pools on the Isle of Skye, Scotland, with their crystal clear blue water and rocky waterfalls, moody and magical lighting, professional photography. Prompt (mid): The vibrant, colorful houses of Cinque Terre, Italy, clinging to a cliffside above the Ligurian Sea, bright sunny day, professional travel photo. Prompt (right): A frozen waterfall in winter, with intricate icicles forming a natural sculpture, cold blue tones, macro details, sharp focus, professional nature photography.

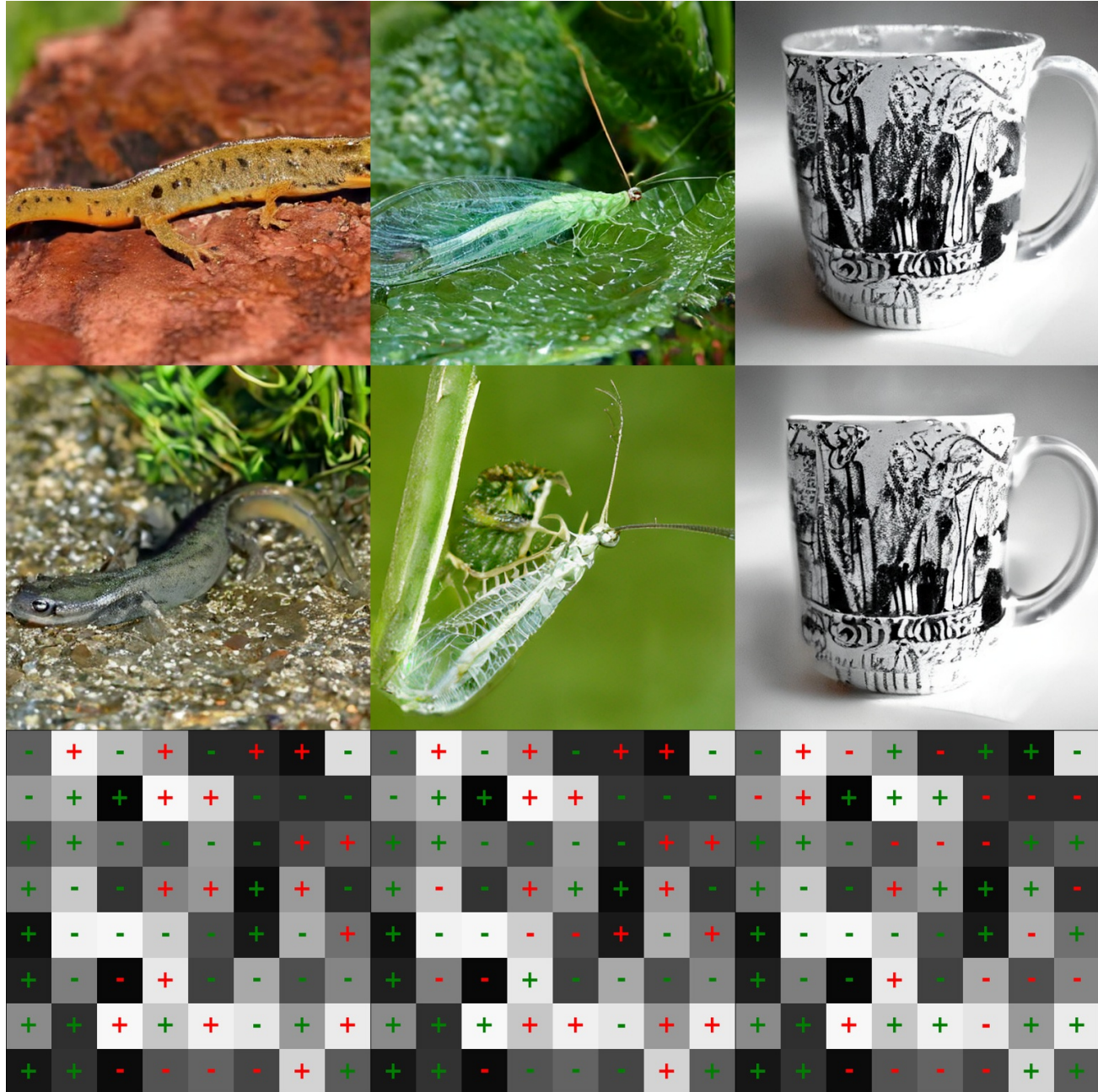


Figure 12. Visualization of EDM2-XS.

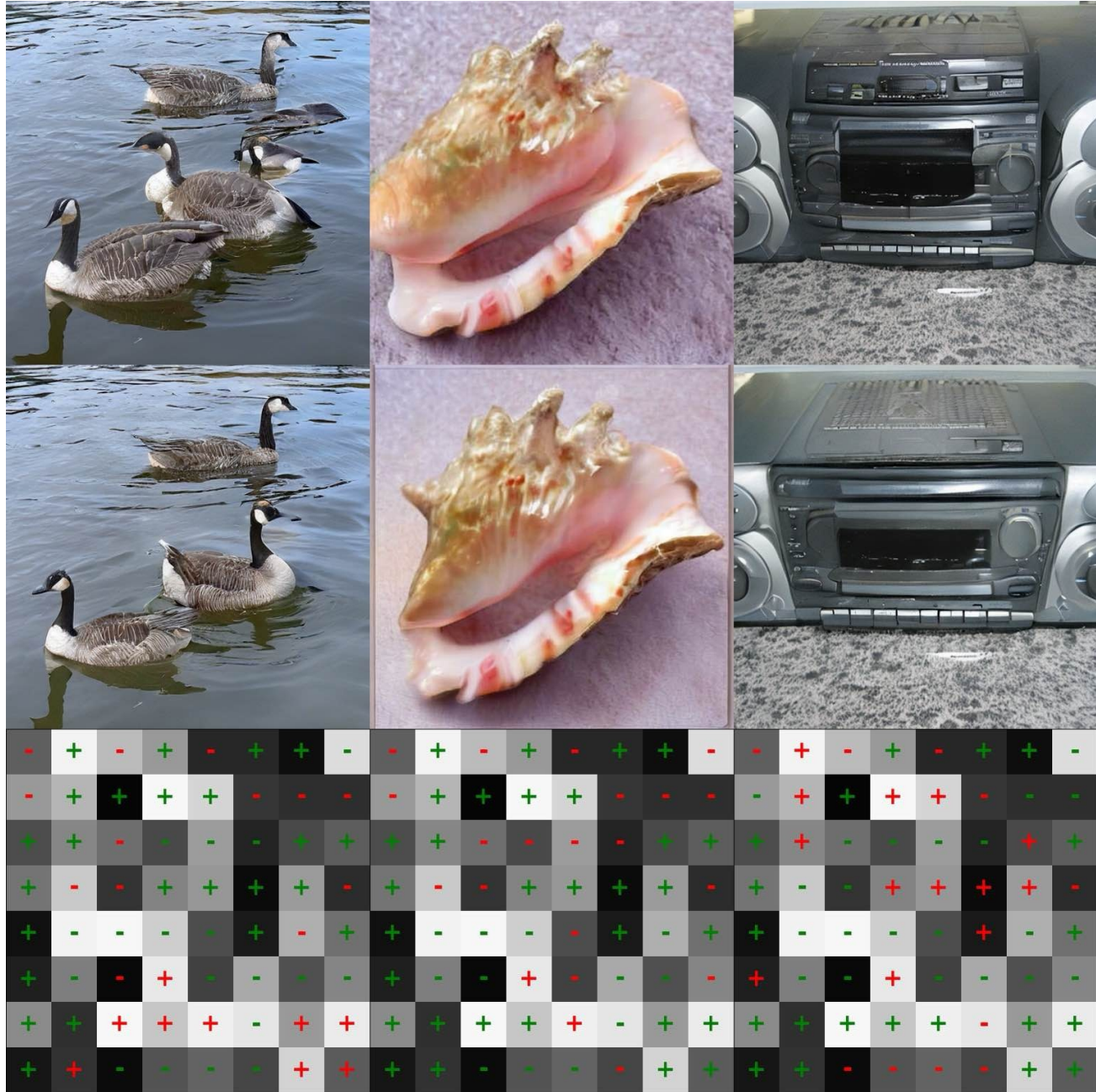


Figure 13. Visualization of EDM2-L.

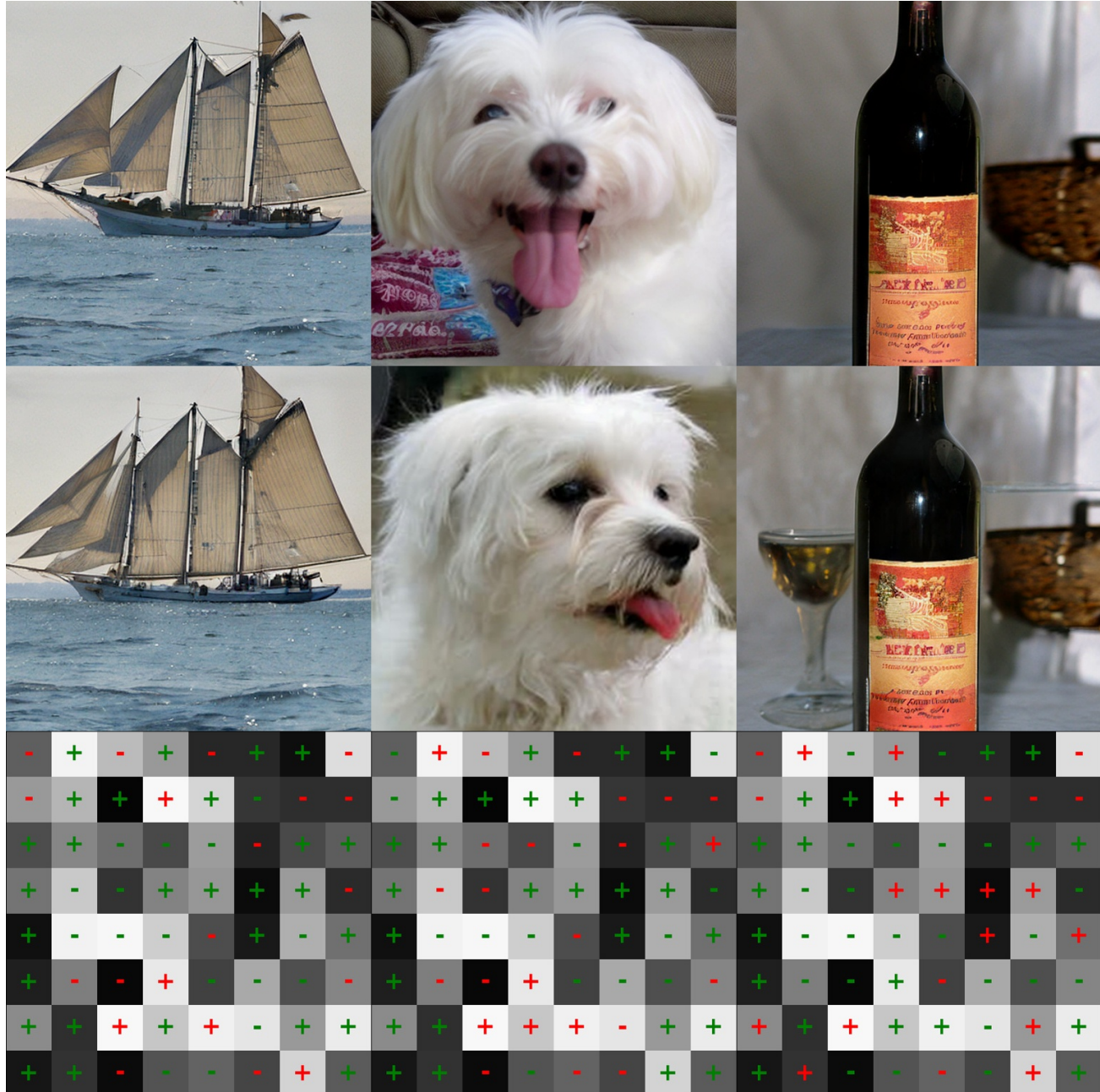


Figure 14. Visualization of EDM2-XXL.

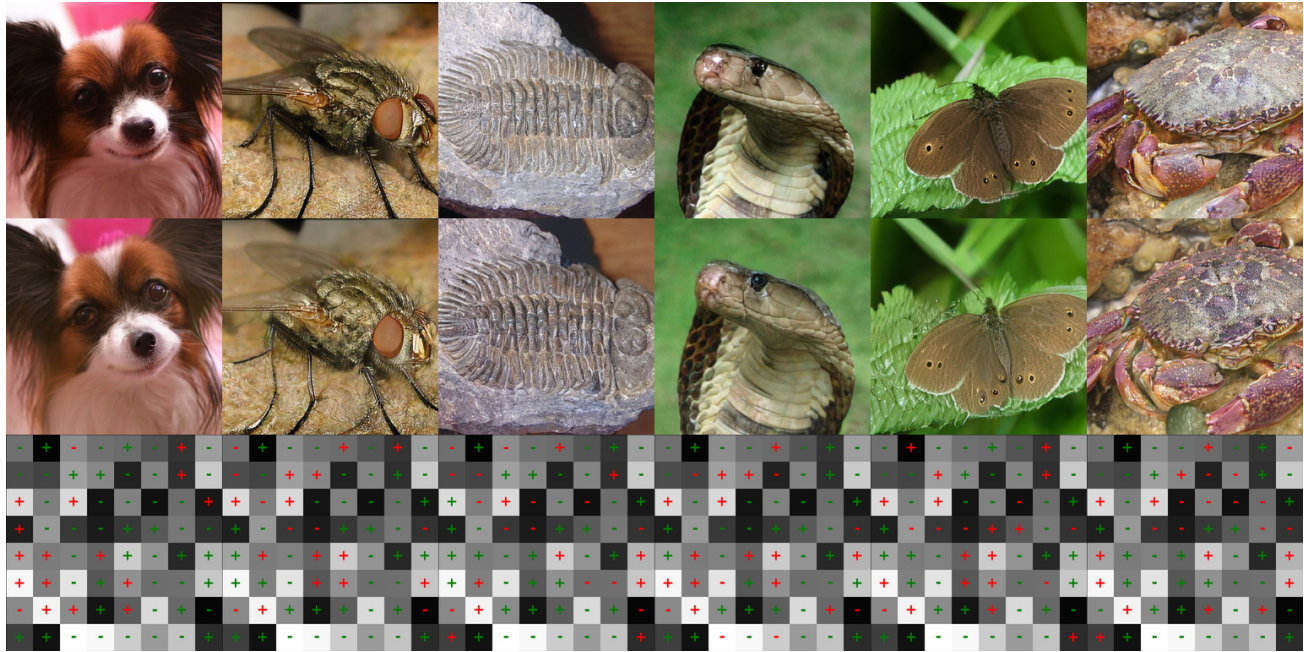


Figure 15. Visualization of VAR-d16.

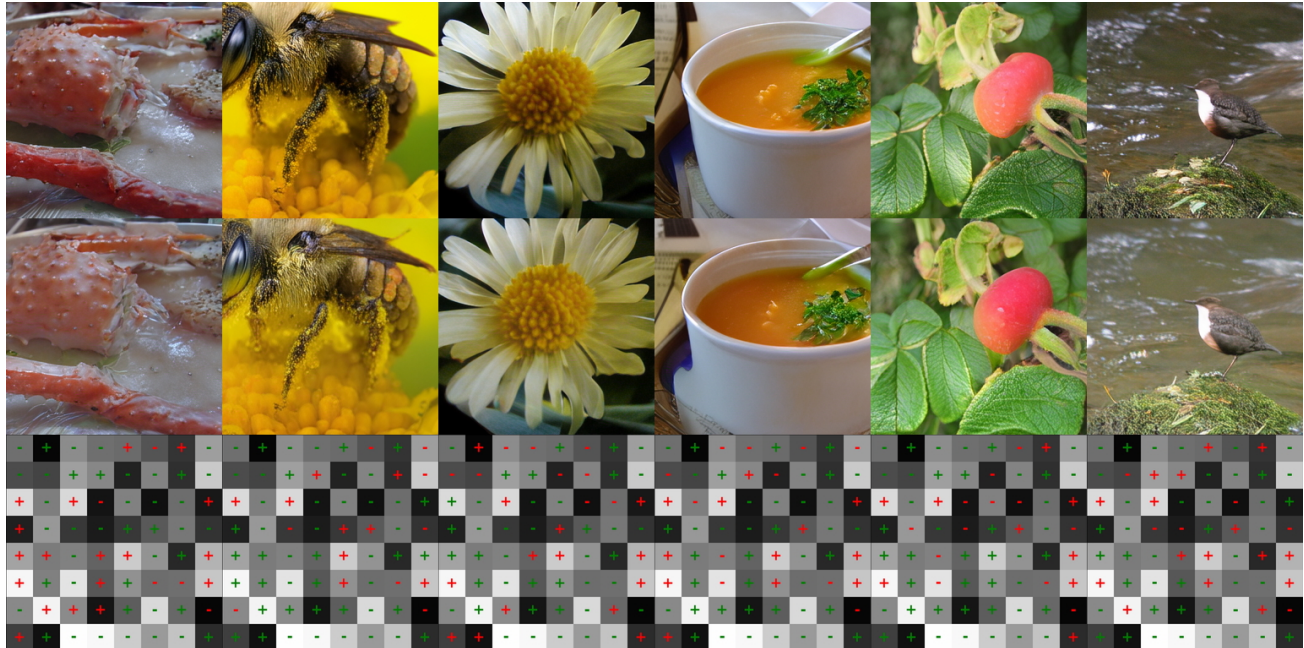


Figure 16. Visualization of VAR-d30.

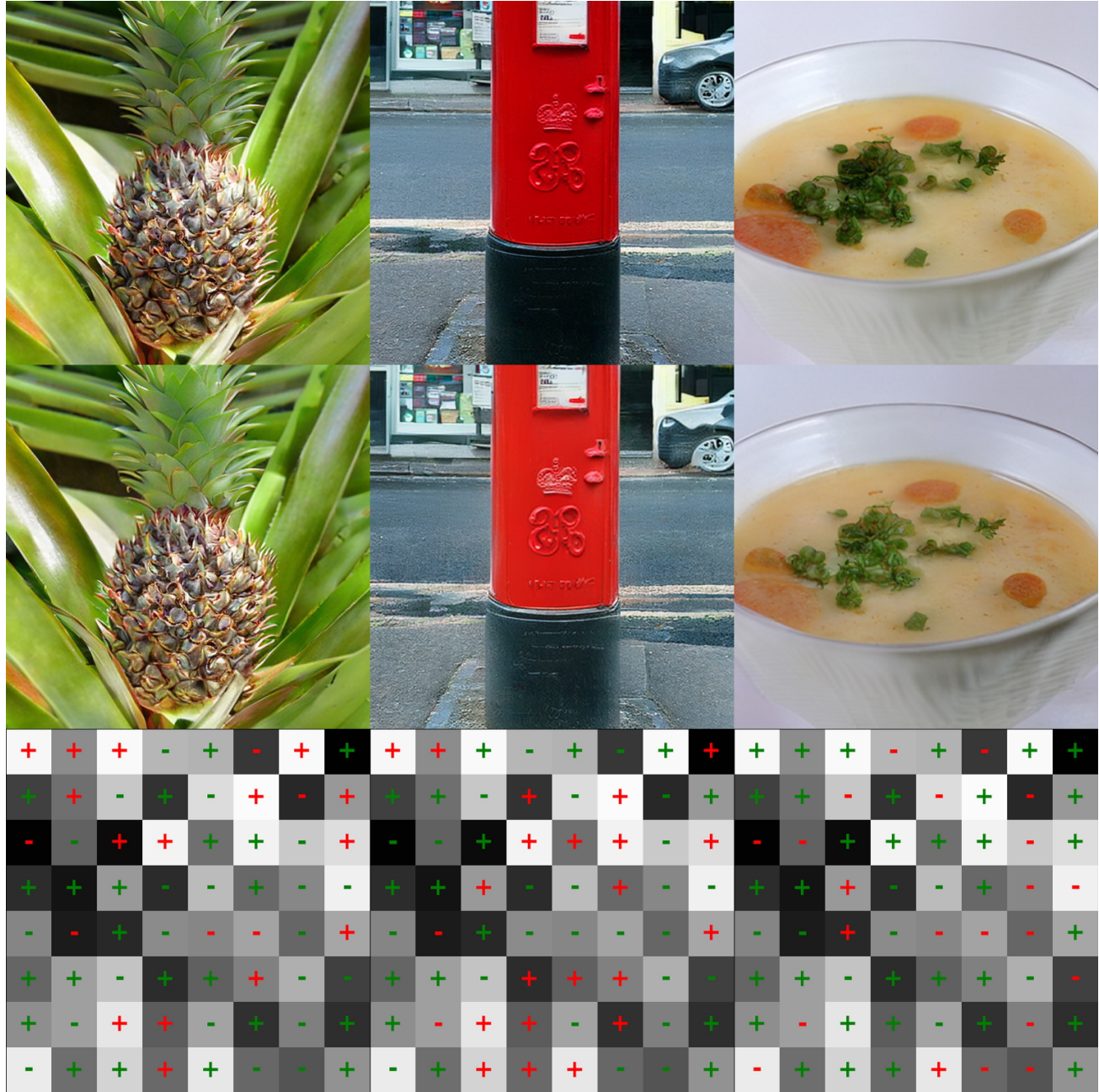


Figure 17. Visualization of VAR-d36.

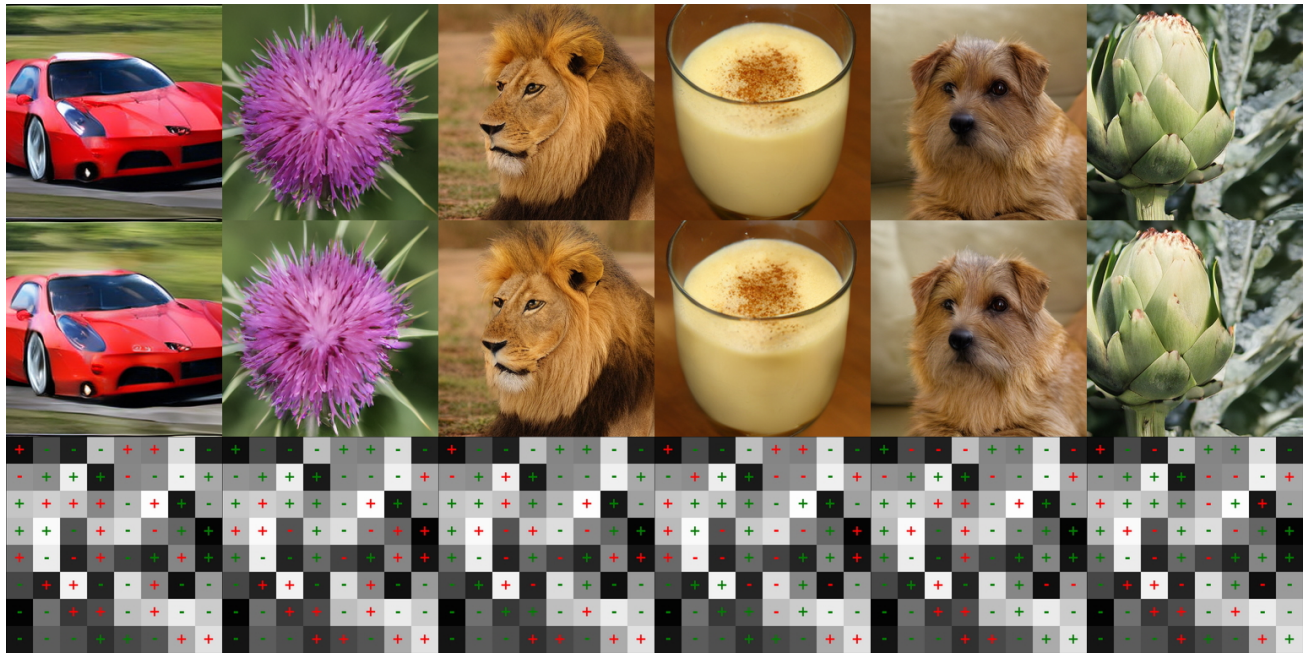


Figure 18. Visualization of MAR-B.

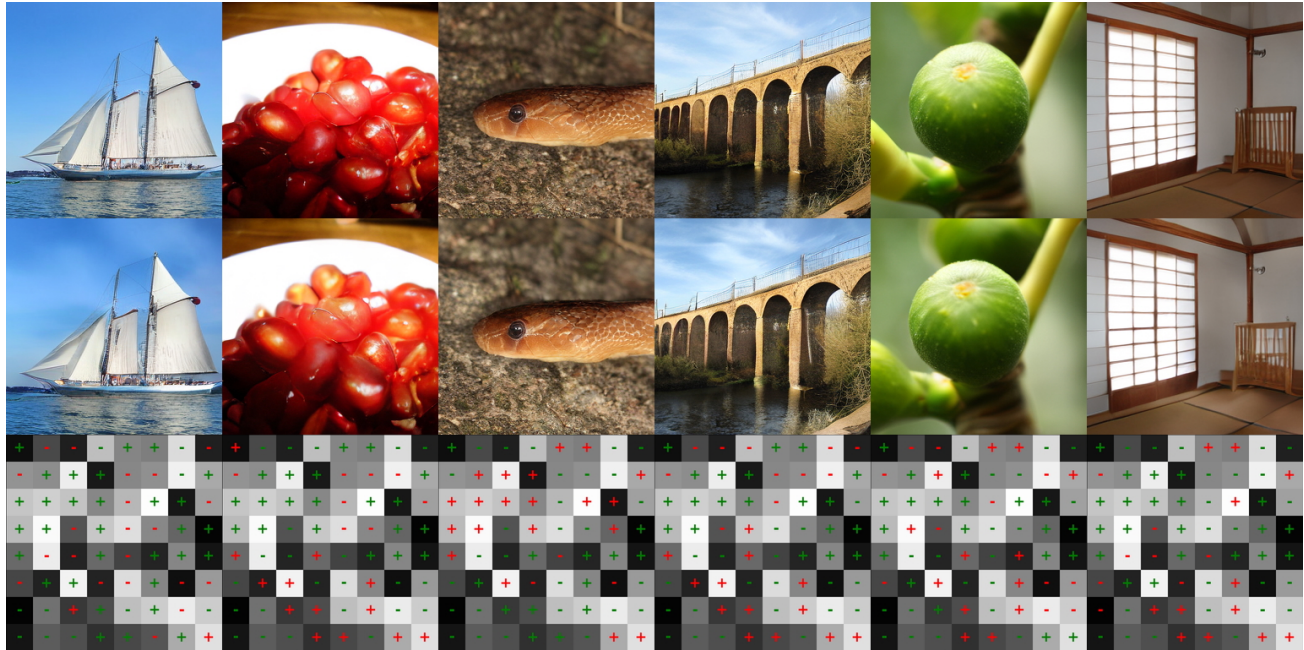


Figure 19. Visualization of MAR-L.

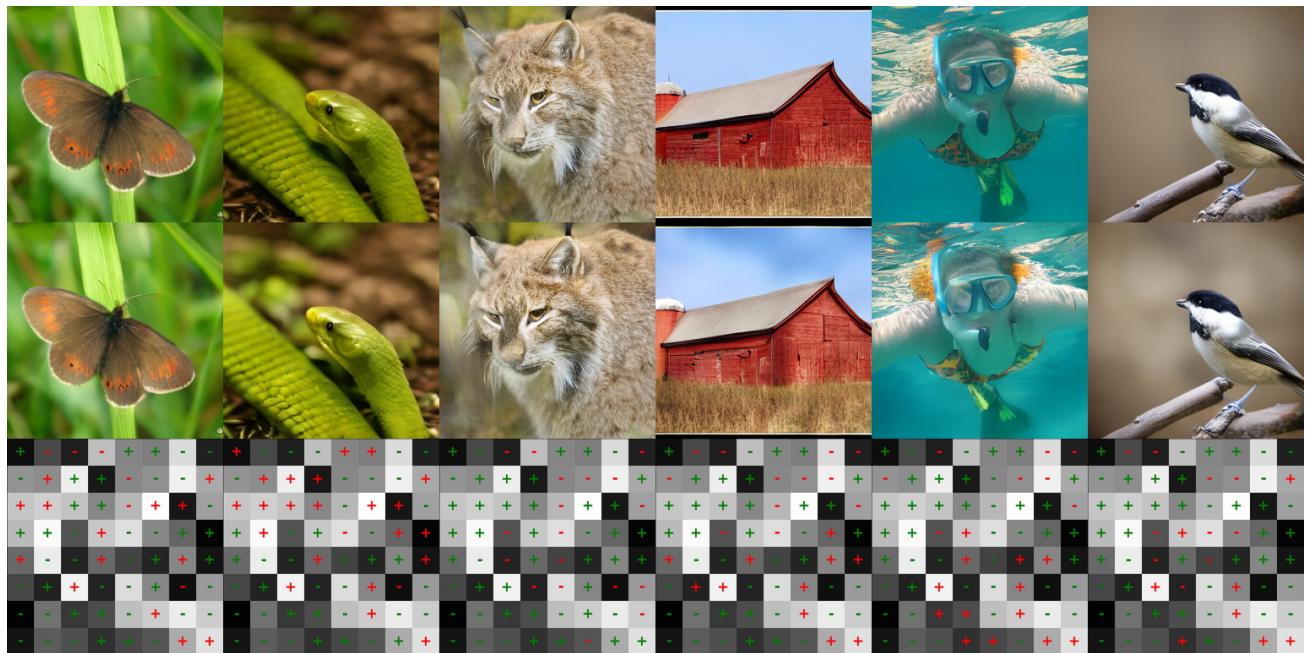


Figure 20. Visualization of MAR-H.

D. Guided Sampling for Latent Diffusion Models

Algorithm 3 introduces a simple version of watermark injection for pixel-space diffusion models. While effective, state-of-the-art diffusion models typically operate in the latent space (Karras et al., 2024b). In these models, the diffusion process unfolds entirely in the latent domain, and the final image is produced by a decoder network DEC that projects the latent representation back into pixel space. It is easy to see that this framework does not affect our watermark detection algorithm. However, the generation procedure in Algorithm 3 requires adaptation. For latent diffusion models, at each sampling step t , we decode the latent vector \mathbf{z}_t into pixel space using the decoder, enabling computation of the penalty term. Since the mapping from a latent vector to its corresponding penalty value is almost everywhere differentiable, we can still compute $\nabla_{\mathbf{z}_t} \text{Penalty}(\text{DEC}(\mathbf{z}_t), \mathcal{W})$, making the guidance possible. The full algorithm for Luminark applied to latent diffusion models is provided in Algorithm 4.

Algorithm 4 Luminark Injection for LDMs

```

1: Input: Denoiser model  $D(\mathbf{z}, \sigma)$ , Decoder  $\text{DEC}$ , diffusion steps  $T$ , noise schedule  $\{\sigma_t\}_{t=0}^T$ , watermark  $\mathcal{W} = (\mathbf{c}, \tau)$ , watermark guidance scale  $s$ , threshold  $T_{\text{match}}$ 
2: repeat
3:   Initialize: sample  $\mathbf{z}_T \sim \mathcal{N}(0, \sigma_T^2 \mathbf{I})$ 
4:   for  $t = T, \dots, 1$  do
5:      $\mathbf{z}_{t-1} \leftarrow \mathbf{z}_t - \left[ \underbrace{\frac{\mathbf{z}_t - D(\mathbf{z}_t, \sigma_t)}{\sigma_t}}_{\text{Denoising Term}} + \underbrace{s \nabla_{\mathbf{z}_t} \text{Penalty}(\text{DEC}(\mathbf{z}_t), \mathcal{W})}_{\text{Watermark Guidance Term}} \right] (\sigma_t - \sigma_{t-1})$ 
6:   end for
7:    $\mathbf{x}_0 \leftarrow \text{DEC}(\mathbf{z}_0)$  ▷ Decode final latent to image
8:    $m \leftarrow \frac{1}{N} \sum_{i=1}^N \mathbb{I}[\text{sgn}(l(\mathbf{p}_i) - \tau_i) = c_i]$  ▷ Compute Match Rate on  $\mathbf{x}_0$ 
9: until  $m \geq T_{\text{match}}$ 
10: return  $\mathbf{x}_0$ 

```

E. Guided Sampling for AR Models

Recent works, including the Vision Autoregressive Model (VAR) (Tian et al., 2024) and Masked Autoregressive Model (MAR) (Li et al., 2024), utilize guidance to enhance the quality of generation. For context, the autoregressive model can be generally formulated as:

$$P(\mathbf{h}_1, \mathbf{h}_2, \dots, \mathbf{h}_T) = \prod_{k=1}^T P(\mathbf{h}_t | \mathbf{h}_{<t}), \quad (9)$$

where $\mathbf{h}_{<t}$ denotes $(\mathbf{h}_1, \mathbf{h}_2, \dots, \mathbf{h}_{t-1})$. In VAR, \mathbf{h}_t corresponds to the intermediate t -th-resolution images in the generation process, whereas in MAR, \mathbf{h}_t is defined as the set of image tokens generated at the t -th step.

In the diffusion paradigm, Watermark Guidance is applied by modifying the denoising term at every step to enforce the luminance constraint, with its core idea being a step-wise modification procedure. Autoregressive models also proceed sequentially, which allows any guidance to be incorporated by adjusting the distribution $p(\mathbf{h}_t | \mathbf{h}_{<t})$ at each step. Since both VAR and MAR operate in the latent space, we adopt the same methodology described in Appendix D: at each step, the latent representation \mathbf{z} is decoded into an image via DEC , then we can obtain $\nabla_{\mathbf{z}} \text{Penalty}(\text{DEC}(\mathbf{z}), \mathcal{W})$. Detailed procedures are outlined in Algorithms 5 and 6, where modifications to the original code are highlighted in blue.

Algorithm 5 Luminark Injection for VAR

```

1: Input: Autoregressive model  $p$ , Decoder  $\text{DEC}$ , watermark pattern  $\mathcal{W} = (\mathbf{c}, \tau)$ , watermark guidance scale  $s$ , label  $y$ ,  

   resolution_scales (e.g.,  $\{1, 2, 3, 4, 5, 6, 8, 10, 13, 16\}$ ), apply_constraint_steps (e.g.,  $\{8, 10, 13, 16\}$ ), guidance steps  $S$ ,  

   threshold  $T_{\text{match}}$ 
2: repeat
3:   Initialize:  $\mathbf{z} \leftarrow \text{embedding}(y)$  ▷ VAR employs conditional generation by default
4:   for  $t = 1, 2, \dots, \text{len(resolution_scales)}$  do
5:      $\tilde{\mathbf{h}}_{t-1} \leftarrow \text{interpolate}(\mathbf{z}, \text{resolution_scales}[t-1])$  ▷ Interpolate  $\mathbf{z}$  to current resolution
6:     Sample next token  $\mathbf{h}_t \sim p(\mathbf{h}_t | \mathbf{h}_0, \mathbf{h}_1, \dots, \tilde{\mathbf{h}}_{t-1})$ 
7:     last_scale  $\leftarrow \text{resolution_scales}[-1]$  ▷ The final image scale (i.e., the scale of  $\mathbf{z}$ )
8:      $\mathbf{z} \leftarrow \mathbf{z} + \text{interpolate}(\mathbf{h}_t, \text{last\_scale})$  ▷ Residual design
9:     if  $t$  in apply_constraint_steps then
10:       $\mathbf{z} \leftarrow \mathbf{z} - \nabla_{\mathbf{z}} \text{Penalty}(\text{DEC}(\mathbf{z}), \mathcal{W})$  ▷ Apply guidance
11:    end if
12:   end for
13:    $\mathbf{x} \leftarrow \text{DEC}(\mathbf{z})$  ▷ Decode final latent to image
14:    $m \leftarrow \frac{1}{N} \sum_{i=1}^N \mathbb{I}[\text{sgn}(l(\mathbf{p}_i) - \tau_i) = c_i]$  ▷ Compute Match Rate on  $\mathbf{x}$ 
15: until  $m \geq T_{\text{match}}$ 
16: return  $\mathbf{x}$ 

```

Algorithm 6 Luminark Injection for MAR

```

1: Input: Autoregressive model  $p$ , Decoder  $\text{DEC}$ , watermark pattern  $\mathcal{W} = (\mathbf{c}, \tau)$ , watermark guidance scale  $s$ , label  $y$ ,  

   ar_step  $T$ , threshold  $T_{\text{match}}$ 
2: repeat
3:   Initialize: mask_steps  $\leftarrow \text{gen\_mask\_order}(T)$  ▷ Random generation order
4:   Initialize:  $\mathbf{z} \leftarrow \mathbf{0}$  ▷ Maintain the generated  $\mathbf{h}$  with corresponding position
5:   for  $t = 1, 2, \dots, \text{ar\_step}$  do
6:     mask_to_pred  $\leftarrow \text{mask\_steps}[t]$ 
7:     Sample next tokens  $\mathbf{h}_t \sim p(\mathbf{h}_t | \mathbf{h}_1, \mathbf{h}_2, \dots, \mathbf{h}_{t-1}, y, \text{mask\_to\_pred})$ 
8:      $\mathbf{z}[\text{mask\_to\_pred}] \leftarrow \mathbf{h}_t$  ▷ Update masked positions in  $\mathbf{z}$ 
9:      $\mathbf{h}_t \leftarrow \mathbf{h}_t - \nabla_{\mathbf{h}_t} \text{Penalty}(\text{DEC}(\mathbf{z}), \mathcal{W})$  ▷ Apply guidance
10:     $\mathbf{z}[\text{mask\_to\_pred}] \leftarrow \mathbf{h}_t$  ▷ Update masked positions in  $\mathbf{z}$ 
11:   end for
12:    $\mathbf{x} \leftarrow \text{DEC}(\mathbf{z})$  ▷ Decode final latent to image
13:    $m \leftarrow \frac{1}{N} \sum_{i=1}^N \mathbb{I}[\text{sgn}(l(\mathbf{p}_i) - \tau_i) = c_i]$  ▷ Compute Match Rate on  $\mathbf{x}$ 
14: until  $m \geq T_{\text{match}}$ 
15: return  $\mathbf{x}$ 

```

F. Description of Baseline Methods

To the best of our knowledge, few studies have investigated watermarking techniques on state-of-the-art autoregressive models, such as VAR (Tian et al., 2024) and MAR (Li et al., 2024). Notable watermarking approaches are specifically designed for diffusion models, such as recent Gaussian-Shading (Yang et al., 2024) and the PRC watermark (Gunn et al., 2024). Therefore, we select these two methods as the baseline.

Both Yang et al. (2024) and Gunn et al. (2024) are developed upon the pioneer Tree-Ring (Wen et al., 2023) approach. The core principle of these methods is to inject a signature into the initial noise during the diffusion process, and subsequently generate the watermarked image by solving the Probability-Flow Ordinary Differential Equation (ODE). The verification process leverages the diffeomorphism property of the ODE: we can use an inverse ODE to reconstruct the initial noise, thereby detecting the watermark's presence. Specifically, the signature in Gaussian Shading consists of noise samples drawn from specific intervals of the Gaussian distribution, while that of PRC-W is defined as the signs of the noise vector. From the description, we can also easily see that this mechanism is specifically designed within the diffusion paradigm and

incompatible with other generative architectures.

Compared with [Yang et al. \(2024\)](#) and [Gunn et al. \(2024\)](#), a key difference in our experimental setup is that we generate a unique watermark for each method and keep it fixed throughout the experiment. In contrast, the experimental setup in [Yang et al. \(2024\)](#) and [Gunn et al. \(2024\)](#) randomly generates a watermark on the fly for each image. Our setting is evidently more practical, as a service provider can realistically maintain only a limited number of keys, which makes reliable detection feasible. By comparison, generating keys on the fly not only incurs significant overhead in maintaining keys but also complicates detection. A notable advantage of this alternative experimental design is that it increases image diversity, which in turn yields substantially lower FID scores. For completeness, we also replicated their experimental setting. Empirically, we observe that the FIDs of all methods are similar and close to the reference.

G. Hyperparameters

G.1. EDM2 Hyperparameters

We conduct experiments on three models from the EDM2 family: EDM2-XXL, EDM2-L, and EDM2-XS. Each model is a latent diffusion model trained on the ImageNet dataset, with images generated at a final resolution of 512×512 .

All models in the EDM2 family utilize a U-Net architecture. For EDM2-XXL, the number of channels is set to 448, and the number of residual blocks per resolution in U-Net is set to 3, resulting in a total of 3.05 billion parameters. For EDM2-L, the number of channels is set to 320, and the number of blocks is set to 3, resulting in a total of 1.56 billion parameters. For EDM2-XS, the number of channels is set to 128, and the number of parameters is 0.25 billion. The diffusion process is performed in the latent space, whose dimensionality is $64 \times 64 \times 4$. Each image is first encoded into this space using a VAE encoder. After the diffusion process, the latent representation is projected back into the pixel space through the corresponding decoder.

We conduct our experiments using the official open-source implementation² and the released pretrained checkpoints. For the diffusion process, we follow the default configuration: the number of diffusion steps is fixed at 32, with $\sigma_{min} = 0.002$, $\sigma_{max} = 80$, and $\rho = 7$, employing Heun’s second-order ODE solver. For our watermark generator, the threshold τ is randomly sampled from a uniform distribution $U(0.4, 0.6)$ to avoid extreme values, and c is randomly chosen from -1 and +1 with equal probability. τ and c are generated and then fixed during each experiment. For watermark injection, the patch size is a key hyperparameter. Choosing a patch size that is too small overly constrains local flexibility, whereas an excessively large patch size degrades detection performance. In all experiments, we therefore fix the patch size to 64×64 for all models, and the total number of patches is 64. The watermark guidance scale (s) controls the strength of the injection during the denoising process. For EDM2-XXL, we set s to be 34.375. For EDM2-L, we set s to be 34.375. For EDM2-XS, we set s to be 34.375. To achieve a false positive rate (fpr) of 1%, we set match rate threshold $T_{match} = 0.61$ using [Algorithm 1](#).

G.2. VAR Hyperparameters

We conduct experiments on three models from the VAR family: VAR-d36, VAR-d30, and VAR-d16. Each model is a latent visual autoregressive model trained on the ImageNet dataset, generating images at a final resolution of 512×512 for VAR-d36, and 256×256 for VAR-d16 and VAR-d30.

All models in the VAR family directly leverage GPT-2-like transformer architecture ([Radford et al., 2019](#)). In VAR-d36, the embedding dimension is 2304, with 36 attention heads and 36 transformer layers, resulting in a total of 2.35 billion parameters. In VAR-d30, the embedding dimension is 1920, with 30 attention heads and 30 transformer layers, resulting in a total of 2.01 billion parameters. In VAR-d16, the embedding dimension is 1024, with 16 attention heads and 16 transformer layers, resulting in a total of 0.31 billion parameters. The generation process is performed in the latent space, whose dimensionality is $32 \times 32 \times 32$ for VAR-d36, and $16 \times 16 \times 32$ for VAR-d16 and VAR-d30. The resolution scales used are $\{1, 2, 3, 4, 6, 9, 13, 18, 24, 32\}$ for VAR-36, while $\{1, 2, 3, 4, 5, 6, 8, 10, 13, 16\}$ for VAR-16 and VAR-30. Each image is first encoded into the latent space using a VQVAE encoder. After the generation process, the latent representation is projected back into pixel space through the corresponding decoder.

We conduct our experiments using the official open-source checkpoint³. Since ([Tian et al., 2024](#)) only released a demo rather than the full sampling code, we re-implemented their method for comparison. For our watermark generator, the threshold τ

²<https://github.com/NVlabs/edm2>

³<https://huggingface.co/FoundationVision/var>

is randomly sampled from a uniform distribution $U(0.4, 0.6)$ to avoid extreme values, and c is randomly chosen from -1 and +1 with equal probability. τ and c are generated and then fixed during each experiment. For watermark injection, we fix the total number of patches to 64 for all models, resulting in a patch size of 64×64 for VAR-36, while 32×32 for VAR-16 and VAR-30. Watermark injection is not applied at all scales. For VAR-16 and VAR-30, the watermark constraint is enforced at the last four resolutions (8, 10, 13, and 16), whereas for VAR-36, the constraint is applied only at the final resolution (32). The watermark guidance scale is fixed at $s = 0.05$ for VAR-16 and VAR-30. For VAR-36, since the guidance is applied only at the final step, we adopt a gradient-descent formulation with a reduced strength of $s = 0.015$, optimizing over 8 steps. To achieve a false positive rate (fpr) of 1%, we set match rate threshold $T_{match} = 0.625$ using Algorithm 1.

G.3. MAR Hyperparameters

We conduct experiments on three models from the MAR family: MAR-B, MAR-L, and MAR-H. Each model is a latent autoregressive model trained on the ImageNet dataset, with images generated at a final resolution of 256×256 .

All models in the MAR family utilize a Transformer (Vaswani et al., 2017) ViT (Dosovitskiy et al., 2020) architecture for token embedding and an additional MLP for the diffusion procedure. MAR-H, MAR-L, and MAR-B, respectively, have 40, 32, and 24 Transformer blocks with a width of 1280, 1024, and 768. The denoising MLP, respectively, has 12, 8, and 6 blocks and a width of 1536, 1280, and 1024. The generation process is performed in the latent space, whose dimensionality is $16 \times 16 \times 16$. Each image is first encoded into this space using a VAE encoder. After the generation process, the latent representation is projected back into pixel space through the corresponding decoder.

We conduct our experiments using the official open-source implementation ⁴ and the released pretrained checkpoints. For the generation process, we follow the default configuration: the number of autoregressive steps is fixed at 256, and the diffusion sampling step is set to 100. For our watermark generator, the threshold τ is randomly sampled from a uniform distribution $U(0.4, 0.6)$ to avoid extreme values, and c is randomly chosen from -1 and +1 with equal probability. τ and c are generated and then fixed during each experiment. For watermark injection, the total number of patches is fixed at 64, yielding a patch size of 32×32 , and the guidance scale is set to $s = 0.015$ across all models. To achieve a false positive rate (fpr) of 1%, we set match rate threshold $T_{match} = 0.61$ using Algorithm 1.

H. Use of Large Language Models (LLMs)

In preparing this manuscript, we used ChatGPT (OpenAI) solely as a writing assistant to improve the readability and fluency of the text. Specifically, the model was employed to polish the language and refine grammar without contributing to the conceptualization, methodology, analysis, or results of this work. All ideas, experiments, and conclusions are entirely the authors' own.

⁴<https://github.com/LTH14/mar>